Chapter 4
Application of Soil Sensing in Precision Agriculture

Sakae Shibusawa, Masakazu Kodaira, Eiji Morimoto, and Minzan Li

Abstract Soil mapping technologies are required to visualize spatial and temporal variability between fields or within field. Proximal and nondestructive soil sensing coupled with GPS using visible and near-infrared (Vis-NIR) spectroscopy or electrical conductivity sensor (soil EC) is a promising approach. A series of tractor-mounted soil-analyzing systems based on Vis-NIR spectroscopy were developed. The structure of the systems is mainly composed of a connection unit (three-point hitch structure), a sensing unit, and a soil penetration part. In the sensing unit, a Vis-NIR spectrometer (NIR enhanced: 310–1100 nm, 3.1 nm/pixel interval), a halogen lamp, thermometers, and a personal computer are installed. The load cell provides cutting resistance measurement and automatic retreat function of the soil-penetrating part due to overloading. In the sensor probe box, a color microcamera head, a radiation/light-concentrating fiber, a displacement meter, and an air blow head are equipped. Estimation models of 33 soil parameters, including moisture content, total carbon, total nitrogen, and soil organic matter, were established with the spectral reflectance data obtained by the tractor-mounted soil-analyzing systems. The result shows the higher multiple calibration accuracy. A smart rice transplanter was developed, which could measure soil EC (apparent electrical conductivity) and topsoil depth. The fertility of the soil varies due to uneven distribution of compost or soil conditioner, and these variations will result in crop lodging at harvest time. The smart rice transplanter developed solves this lodging problem with soil EC data and performs real-time variable fertilizer application.

Keywords Proximal soil sensing · Vis-NIR spectroscopy · Soil mapping · Soil electrical conductivity · Soil sensor

S. Shibusawa · M. Kodaira (✉)
Tokyo University of Agriculture and Technology, Tokyo, Japan
e-mail: kodaira@cc.tuat.ac.jp

E. Morimoto
Tottori University, Tottori, Japan

M. Li
China Agricultural University, Beijing, China

4.1 Tractor-Mounted Soil Analysis System Based on Vis-NIR Spectroscopy

4.1.1 Soil Sensing Instruments Based on Vis-NIR Spectroscopy

Precision agriculture (PA) aims to improve agricultural profitability and productivity (yield, quality, farming, etc.), as well as protecting environment. It has been enabled by the rapid development and spread of GNSS (Global Navigation Satellite System), GIS (Geographic Information System), and ICT (Information and Communications Technology).

To practice PA, the required technologies include field mapping technology to visualize spatial and temporal variability between fields or within field, variable-rate technology to perform farming work corresponding to the variability, and decision support system to solve complex problems and requirements. Especially, field mapping technology is the basis of PA. The technological feature of PA is to accurately record the spatial and temporal variability of soil, crop, yield, etc., to realize site-specific field management at low cost using field maps.

In terms of soil analysis, soil samples are collected from the field and analyzed by official method. The problems are the cost, analysis period, and labor for a large number of soil samples with location information collected for analysis of multiple properties to support the PA practice, and few growers are willing to adopt soil analysis for each cropping. The analysis period has been shortened compared to the official method by the development of a simple soil analysis method, which contributed to the improvement of soil analysis business. However, when crops with a short period from harvesting to sowing were cultivated in same field, it was difficult to plan and distribute fertilizer based on the soil analysis result using soil samples collected after harvest. The problems of labor and cost consuming on the grower side have not been improved.

To overcome these problems, development of soil sensing devices has been carried out using electrical, electromagnetic, acoustic, pneumatic, and optical technologies. It has been reported that spectroscopic technology using visible (Vis), near-infrared (NIR), and infrared (IR) soil reflectance is nondestructive, rapid, and cost-effective, with high accuracy compared to other soil sensing technologies (Adamchuk et al. 2004). The purpose to introduce spectroscopic technology in soil analysis is to improve price-performance ratio, which has more rapid and higher efficiency than the official and simple soil analytical method. In addition, the predicted values are required to be absolute quantitative values, with the accuracy at a level equivalent to the official method. The mainstream of soil spectroscopic analysis is to measure the soil diffuse reflectance spectra using a spectrophotometer installed in laboratory. As a result, the problems on the analysis business side have been improved. But the problems on the grower side, such as labor consuming in soil sampling with location information and sample drying and 2 mm sieving pretreatment work, have not yet been considered. The new problems are that the instrument is expensive, and it is necessary to analyze regression coefficient for each soil

type and each soil property. The number of soil properties is limited, and accuracy is low for nitrogen, phosphorous, and potassium which are required for fertilization design (Dalal and Henry 1986; Matsunaga and Uwasawa 1992a, b, 1993; Chang et al. 2001; Viscarra Rossel et al. 2006).

In order to measure a large amount of soil diffuse reflectance spectra with position information using a spectrophotometer without soil sample collection, field measurement-type (field-type hereinafter) spectrophotometers have been developed which can simultaneously measure the soil diffuse reflectance and position information in a field. When measuring raw soil sample spectra, the difference in water content greatly influences the spectra in the infrared region. Therefore, the field-type spectrophotometers have been developed which equipped with spectroscopic sensors sensitive in Vis-NIR wavelength range that is less affected by soil moisture (Shibusawa et al. 2000a, b; Mouazen et al. 2007; Christy 2008). As a result, the problems on both grower and analysis business sides have been improved. However, as "new problems" to the laboratory spectrophotometer, the countermeasures for that the field-type spectrophotometer cannot be used in fields such as slope, orchards, and forest have not been considered. In field measurement, diffuse reflectance spectra from other substances than soil, such as gravel and crop residues, may cause prediction errors. In addition, the soil diffuse reflectance spectra used to estimate the regression coefficient in previous studies were measured from dried and 2 mm sieved soil. The diffuse reflectance spectra of raw soil measured in a field have to be analyzed using a moisture correction coefficient (Christy 2008; Mouazen et al. 2014). In addition, the estimation errors of the regression coefficient and the moisture correction coefficient have been the factors that reduced the prediction accuracy.

The field-type spectrophotometer is useful as the field soil mapping technology. But the mainstream is to use interpolation methods in commercially available software such as GIS and Excel and the visualization method by grid-like soil mapping (Shibata 1999; Toriyama 2001; Umeda et al. 2011; Kuang and Mouazen 2013). However, the software installation/maintenance is expensive, and data transfer, conversion, and the setting process to display soil map are complicated. The variability status of multiple soil properties is difficult to confirm with growers immediately after the field observation, so it is lack in speed and convenience.

The soil property analyses for soil mapping are soil diagnostic properties (chemical, physical, and biological) that are necessary for crop production. There are more than 20 chemical properties including general properties, trace elements, and nitrogen. In terms of physical properties, besides soil dry density which is important in fertilization design, soil textures (sand, silt, and clay) are indispensable for determining soil fertility. The biological properties have microorganisms and nematodes which are useful information. But types of them are countless, and the analytical method and cultivation guideline are not established. The microorganism in soil decompose organic component into nutrients that can be used by crops and prevent failures, improve physicochemical and biological properties of soil, improve crop productivity and quality, and purify the soil. Therefore, it is becoming an important farming decision information after the chemical fertilizer. In general, the purpose of soil analysis is to estimate the input of chemical fertilizer necessary for crop

production while reducing the environmental impact, and three properties, nitrogen, phosphorous, and potassium, are the target properties. The reason why multi-property soil analysis is recommended is due to the fact of "Dobeneck's barrel" (Hans Arnold von Dobeneck) which proposed that crop growth is governed by the scarcest resource. Or the "Liebig's law of the minimum" by Justus von Liebig, which suggests that crop growth rate and yield are dictated not by total nutrients available but only affected by the scarcest nutrient that provided to the crop (limiting factor). In addition, the absorption of nutrients by crops is a synergistic effect promoted by other nutrients (when present in an appropriate amount), or when a certain nutrient is excessive, it may be an antagonist that suppresses or inhibits the absorption of other coexistence nutrients. These effects are also necessary to be considered. If it becomes possible to provide high-resolution soil maps rapidly with multiple properties, field management using right material with right amount at right time and location will be possible, which will be the basis for preventing excessive application of agricultural materials. Also, since various types of soil property maps are required according to the cultivation purposes of growers, the nondestructive prediction technology based on soil diffusion reflection spectra, which can provide multiple prediction values from a single measurement, is indispensable in soil sensing device.

The results of soil sensing are not only used as field mapping technology for PA but also contribute to soil/field management in good agricultural practice (GAP) which established standards and procedures for food security and provide field information for integration/aggregation, consolidation of fields, and reuse of abandoned land. The 70% use of total freshwater in agriculture is an urgent need for improvement, and soil maps of moisture and physical property are used as consensus building information to allocate freshwater resources efficiently and effectively (Hedley and Yule 2009; Mouazen et al. 2014). This is a contribution to the Sustainable Development Goals (SDGs: 1, 2, 12, 13, and 15) to realize a sustainable world (Ministry of Foreign Affairs of Japan 2018). As one of the countermeasures against global warming, the carbon farming (Australian Government 2011) assesses the ability of soil carbon sequestration. The carbon credit trading conducted by the Chicago Climate Exchange based on Clean Development Mechanism (CDM) is expected to be a source of income of growers.

4.1.2   Tractor-Mounted Soil Analysis Systems

There are potable and tractor-/vehicle-mounted devices that can predict physio-chemical soil properties from diffuse reflectance spectra measured in a field. It was USDA (US Department of Agriculture) (Sudduth and Hummel 1993) that made it possible to continuously measure diffuse reflectance spectra in a field by installing a spectrophotometer on a tractor or vehicle and after that the Tokyo University of Agriculture and Technology (TUAT, Japan) in 1999 (Shibusawa et al. 1999) and Catholic University of Leuven (CU of Leuven, Belgium) (Mouazen et al. 2005) in

2005. Veris Technologies (USA) in 2008 (Christy 2008), Poznan University in 2013 (Poland) (Wojciechowski and Czechlowski 2013), Jacto (Brazil) in 2013, and University of Bonn (Germany) in 2015 (Rodionov et al. 2015) developed the test device, as shown in Table 4.1.

The measurement wavelength range of the USDA's device was 1630–650 nm, the observation depth was 0.35–0.50 m, the observation speed was 0.65 m/s, and the method to estimate regression coefficients was partial least square regression (PLSR). The target soil properties were cation exchange capacity (CEC), organic matter (organic carbon), and soil water content. The prediction accuracy by laboratory measurement (using dry and moist soil) was $R^2 = 0.85$–0.96. But the accuracy

Table 4.1 Comparison of tractor-/vehicle-mounted spectrophotometer

| Authors | Equipment (spectrometer) | Field measurement | | Spectra data for calibration | | Multivariate analysis software |
		Soil depth (m)	Speed (m/s)	Measurement location	Soil condition	
Sudduth and Hummel (1993), USDA	Prototype portable NIR spectrophotometer	0.035~0.05	0.65	Lab	Dry	The Unscrambler
Shibusawa et al. (1999, 2000a, b) and Imade Anom et al. (2001), TUAT	RTSS-01 (MMS 1 and MMS)	0.15, 0.20~0.25	0.28 0.28	Field	Fresh	The S-Plus data analysis
Mouazen et al. (2005, 2007), CU of Leuven	Fiber-type NIR spectrophotometer (Corona 45: MMS 1 and MMS)	0.15	0.42	Lab	Day	The Unscrambler Ver.7.8
Christy (2008), Veris Technologies	On-the-go spectrophotometer (NIR-128L-1.7-USB)	0.07	1.67	Lab	Dry	LabVIEW
Marín González et al. (2013)	Fiber-type NIR spectrophotometer (AgroSpec: MMS 1 and MMS)	0.15	0.83	Lab	Dry	The Unscrambler Ver.7.8
Wojciechowski and Czechlowski (2013), Poznan University	The combined soil measurement system (AgroSpec: MMS 1 and MMS)	–	–	Lab	Dry	The Unscrambler X
Jacto	Jacto Soil Sensor (Corona 45: MMS 1 and MMS)	–	–	Field	Fresh	The Unscrambler Ver.9.8
Rodionov et al. (2015), University of Bonn	Mobile measuring chamber (AgroSpec)	0.05	0.83	Lab	Dry	ParLes 3.1

extremely decreased when measured in a field while moving. It has been reported that the cause was due to the variations in the height of the observation surface and the sensor during the measurement. The purpose of raw soil diffuse reflectance spectra measurement is to obtain prediction values of soil physicochemical properties to create soil maps. However, there was no mechanism equipped to link the location information to the measured data, which did not lead to soil mapping.

The measurement wavelength range of the TUAT's device was 400–1700 nm, the observation depth was 0.30 m, and the observation speed was 0.05 m/s. The soil at the spot where the soil diffuse reflectance spectra were measured in the field was collected, and the reflectance spectra of the raw soil were measured in laboratory using a spectrophotometer (Shimadzu, UV3100). The equivalence of the two measurements was confirmed with correlation coefficient $R = 0.98$. The target properties were electric conductivity (EC), pH, nitrate nitrogen, soil water content, and soil organic matter. The method to estimate regression coefficient adopted single regression, and the accuracy from the spectra measured while moving was $R = 0.44-0.93$. Toward the problems of the USDA's device, Shibusawa et al. (1999) combined the tip of a subsoiler, which could reduce soil resistance and stably operate even at high speeds, with a chisel which was superior in penetration and crushing even in hard field and equipped with a sensor head. The variation in the height of the observation surface and the sensor was suppressed, and stable diffuse reflectance spectra acquisition was successfully conducted. In addition, RTK-GPS (Real-Time Kinematic-Global Positioning System) was installed to link "time and location" to "diffuse reflectance spectra." This made it possible to link position information to the prediction value calculated from the raw soil diffuse reflectance spectra. Since then, the developed devices have been equipped with DGPS (differential GPS) system in addition to the RTK-GPS system.

The measurement wavelength range of the CU of Leuven's device was 306.5–1710.9 nm, the observation depth was 0.15 m, the observation speed was 0.33 m/s, and the regression coefficients were estimated by PLSR (Mouazen et al. 2005, 2007). The target property was soil water content, with $R = 0.98$. For the regression coefficient estimation, a total of six types of soil diffuse reflection spectra were measured by adding water to dry soil from 0 to 0.25 kg/kg (0.05 kg/kg interval). The soil diffuse reflection spectra measured from a field were not used in the estimation of regression coefficient.

The measurement wavelength range of the Veris Technologies' device was 950–1650 nm (Christy 2008), the observation depth was 0.07 m, the observation speed was 1.67 m/s, and the regression coefficients were estimated by principal component regression (PCR). The target soil properties were lime, organic carbon, exchangeable potassium, LBC (lime buffer capacity), soil water content, magnesium, manganese, available phosphorus, pH, and zinc. The soil diffuse reflectance spectra used in the regression coefficient estimation were based on dry soil spectra measured in laboratory. The highest prediction accuracy was organic carbon with $R^2 = 0.67$. For the diffuse reflectance spectra measured in a field, they reduced the prediction error caused by moisture variation by previously analyzing a moisture correction model based on spectra difference between dry soil and moist soil.

The measurement wavelength range of the Poznan University's device was 400–1270 nm; the observation depth was 0.05 m; the observation speeds were 0.05, 0.07, and 0.1 m/s; and the regression coefficient was estimated by PLSR (Wojciechowski and Czechlowski 2013). The target property was soil water content. The accuracies were $R^2 = 0.87–0.89$ at constant and mixing speed.

The measurement wavelength range of the Jacto's device was 400–700 nm, the observation depth was 0.06 m, the observation speed was 0.56 m/s, and the regression coefficients were estimated by PLSR. The target soil properties were pH, CEC, exchangeable potassium, exchangeable calcium, and available phosphorous.

The measurement range of the University of Bonn's device was 410–2300 nm, the observation depth was 0.05 m, the observation speed was 0.83 m/s, and the regression coefficients were estimated by PLSR (Rodionov et al. 2015). The target soil properties were soil organic carbon and soil water content. The R^2 were 0.84 and 0.96, respectively. Although the observation speed was the highest, the moving was temporarily stopped when measuring the diffuse reflectance spectra.

The most used field spectrometers in the devices were MMS and MMS1 (Table 4.1). The highest observation speed at the maximum observation depth of 0.15 m was 0.83 m/s. The diffuse reflectance spectra used to estimate the regression coefficient were mostly based on dry soil in laboratory. The Unscrambler was used as the multivariate analysis software, and PLSR was used as the analysis method. The target soil properties in previous studies included nitrogen, phosphorus, and potassium. But the ranks of the regression coefficient were low, at C and D. The ranks were A and B only for soil water content, soil organic matter, and organic carbon (Table 4.2).

The commercialization of TUAT's device was performed by the Shibuya Machinery Co., Ltd. (Shibuya Seiki Co., Ltd. at present). The measurement properties were soil water content, soil organic matter, total nitrogen, and EC. The general regression coefficient (which does not depend on the soil type and various component concentrations) was not provided. The device commercialized by the Veris Technologies can perform soil mapping for soil organic matter and soil physical properties.

The problem is that it is necessary to analyze moisture correction equation when estimating regression coefficient using the diffuse reflectance spectra of dry soil. Moreover, high-accuracy, multi-property regression coefficient estimation has not been achieved.

4.1.3 Soil Analysis System (SAS) Series

The development of real-time subsoil optical sensor was started in 1997, and joint research was started in 1998 between the TUAT and Omron Corporation, Japan. The prototype was completed in 1999. A 01 model equipped with two spectrometers of Vis-NIR range was developed in 2001, and 02 model of nine-wavelength spectroscopic types (552, 651, 738, 811, 926, 1003, 1303, 1457, 1650 nm) was

Table 4.2 Properties and prediction accuracy of tractor-/vehicle-mounted spectrophotometer

Items	Wavelength (nm)	Analysis method (F)	N	RMSE	R^2	RPD	Rank	Authors
pH	400–1700	SMLR	15	0.16	0.58	1.25	E	Imade Anom et al. (2001)
	306–1710	PLSR (12)	295	0.22	0.71	2.14	C	Mouazen et al. (2007)
	920–1718	PCR	106	0.44	0.62	1.64	D	Christy (2008)
	400–2100	PLSR	160	0.40	0.79	2.16	C	Marín González et al. (2013)
Available phosphorus	920–1718	PCR	116	30.0	0.80	2.24	C	Christy (2008)
	306–1710	PLSR (9)	175	1.35	0.69	1.80	D	Mouazen et al. (2007)
Exchangeable potassium	920–1718	PCR	106	107	0.60	1.54	D	Christy (2008)
Exchangeable magnesium	920–1718	PCR	107	85.0	0.73	2.07	C	Christy (2008)
	400–2100	PLSR	160	0.38	0.69	2.44	C	Marín González et al. (2013)
Exchangeable calcium	920–1718	PCR	105	750	0.82	2.32	C	Christy (2008)
	400–2100	PLSR	160	22.1	0.89	0.83	E	Marín González et al. (2013)
Soluble zinc	920–1718	PCR	93	0.62	0.48	1.37	E	Christy (2008)
Easily reducible manganese	920–1718	PCR	110	34.0	0.40	1.27	E	Christy (2008)
Nitrate nitrogen	400–1700	SMLR	15	4.74	0.54	1.83	D	Imade Anom et al. (2001)
Cation exchange capacity	1630–2650	PLSR (10)	30	3.91	0.85	–	–	Sudduth and Hummel (1993)
	400–2100	PLSR	160	1.77	0.58	1.54	D	Marín González et al. (2013)
Electrical conductivity	400–1700	SMLR	15	41.7	0.65	1.10	E	Imade Anom et al. (2001)
Moisture content	1630–2650	PLSR (10)	30	1.69	0.96	–	–	Sudduth and Hummel (1993)
	400–1700	SMLR	15	3.11	0.66	1.83	D	Imade Anom et al. (2001)
	306–1710	PLSR	348	0.02	0.89	3.00	B	Mouazen et al. (2007)
	920–1718	PCR	105	2.80	0.65	1.75	D	Christy (2008)
	400–2170	PLSR	–	2.24	0.89	–	–	Wojciechowski and Czehlowski (2013)
	410–2300	PLSR	120	1.99	0.96	5.03	A	Rodionov et al. (2015)

(continued)

Table 4.2 (continued)

| Items	Wavelength (nm)	Analysis method (F)	N	RMSE	R^2	RPD	Rank	Authors
Soil organic matter	400–1700	SMLR	15	0.56	0.65	1.86	D	Imade Anom et al. (2001)
	920–1718	PCR	106	0.40	0.80	2.20	C	Christy (2008)
Total carbon	306–1710	PLSR	173	0.27	0.73	1.92	D	Mouazen et al. (2007)
Soil organic carbon	1630–2650	PLSR (10)	30	0.26	0.85	–	–	Sudduth and Hummel (1993)
	410–2300	PLSR	120	0.73	0.84	2.53	B	Rodionov et al. (2015)

N number of samples, *PCR* principal component regression, *RMSE* root mean square error, *RPD* residual prediction deviation (standard deviation/RMSE). Rank (Kuang et al. 2012): A (excellent), B (good), C (approximate quantitative prediction), D (distinguish between high and low), E (not usable)

developed in 2002 (Shibusawa et al. 2000a, b; Bodun et al. 2000; Imade Anom et al. 2001; Kaho et al. 2004; Shibusawa et al. 2005; Roy et al. 2006). Patents associated with the device development (Japanese Patent Application No. Hei10-108862, No.2000-604663, No. 2001-322755, and No. 2002-169192) were transferred from the Omron Corporation to TUAT, and the license and technology were transferred to the Shibuya Machinery Corporation. In 2004, a promotion model of the tractor-mounted soil analysis system (SAS1000[1]) (Fig. 4.1) was developed (Shibuya Machinery Co. Ltd. 2004; Shibusawa et al. 2010; Kodaira and Shibusawa 2013, 2016). SAS is custom-made systems, which have specification for large-scale field (SAS2000), specification for paddy field (SAS2500) (Fig. 4.2) (Kodaira and Shibusawa 2018), specification for woodlot (SAS2600), and specification with self-propelled lightweight (SAS3000) (Fig. 4.3). Since no regression coefficient was provided for soil property, the challenge is to secure human resources who can measure soil diffuse reflectance spectra and physicochemical properties and introduce and operate software such as multivariate analysis and soil mapping.
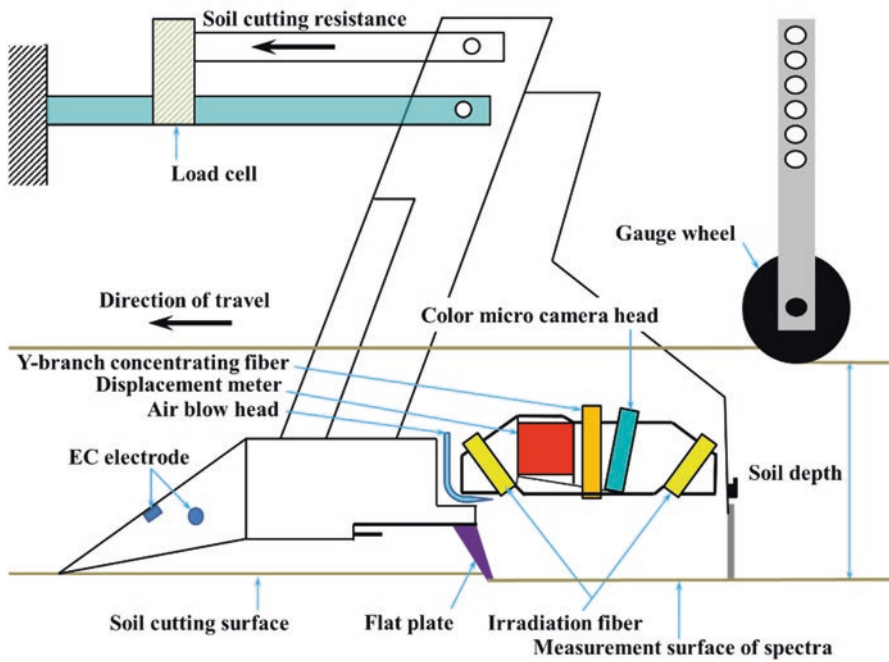
(1) SAS1000

SAS1000 (Fig. 4.1) is composed of a connection unit (three-point hitch structure), a sensing unit, and a soil penetration part (Fig. 4.1b), and the weight is 550 kg. In the sensing unit, Carl Zeiss's Vis-NIR spectrometers (MMS1 NIR enhanced: 310–1100 nm, 3.1 nm/pixel interval), a halogen lamp (Ushio Electric Co., Ltd., JCR15V150WBAL), thermometers (external air, spectrometer, control panel), and a personal computer (PC) are installed. The soil penetration part has vertical and horizontal cutting blades for soil cutting and removal and a chisel plow with a

---

[1] *Disclaimer*: Commercial products are referred to solely for the purpose of clarification and should not be construed as being endorsed by the authors or the institution with which the authors are affiliated.
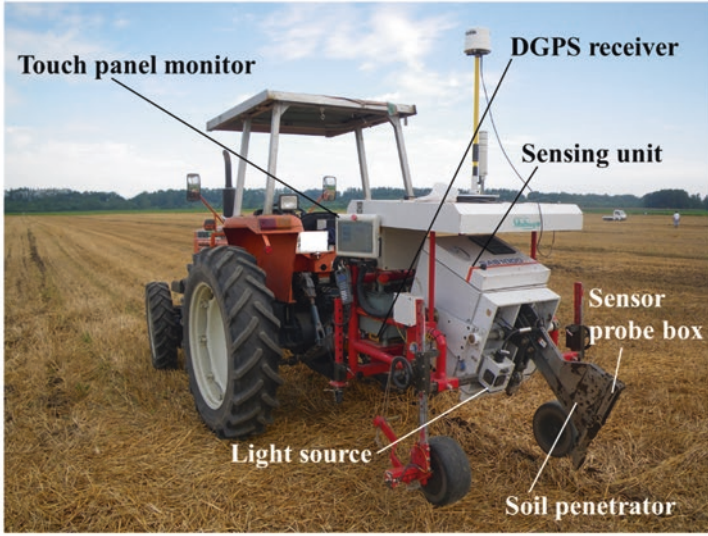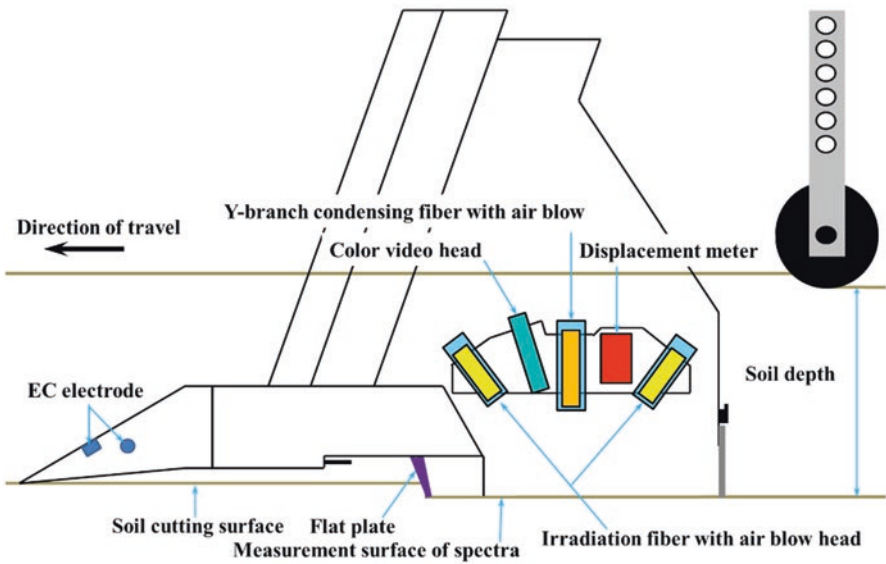
Fig. 4.1 Soil analysis system SAS1000 (**a**) SAS 1000 system, (**b**) Cross section of soil-penetrating part. (Shibusawa et al. 2010)

(a)

(b)

Fig. 4.2 Soil analysis system SAS2500 (**a**) System SAS2500 (**b**) Cross section of soil-penetrating part

Fig. 4.3 Soil analysis system SAS3000

sensor probe box. The load cell provides cutting resistance measurement and automatic retreat function of the soil-penetrating part due to overloading. In the sensor probe box, a color microcamera head (Toshiba Corporation, IK-UM44H), a radiation/light-concentrating fiber (Sumitomo Electric Industry Co., Ltd., GeO$_2$, F-doped quartz system), a displacement meter (Omron Corporation, ZX LD 100), and an air blow head are equipped. Image of the observation surface, Vis-NIR diffuse reflectance spectra, and distance to the observation surface can be obtained without contact with the soil. The soil penetration part is driven by a hydraulic system and a remote controller using tractor PTO as the power source. For location information, it was equipped with a DGPS receiver (Trimble Navigation Limited, DSM132) with horizontal measurement accuracy of less than 1 m. An inverter generator dedicated to SAS (Honda Motor Co., Ltd.) is installed on the tractor body. The observation speed is 0.28–1.12 m/s, the observation depth is 0.15–0.30 m (0.05 m interval), and the measurement interval can be arbitrarily set at 3 s and over (Shibuya Machinery Co. Ltd 2004; Shibusawa et al. 2010).

(2) SAS2500

SAS2500 (weight 660 kg) has been produced under the funding of a Japanese national grant program adopted in 2012 (Fig. 4.2). The different specifications from SAS1000 are that a radiation fiber with air blow head and a Y-branch light-concentrating fiber are used. The microcamera was changed to a video camera. The drive of the soil-penetrating part was changed to a hydraulic system (1 system, 3/8-inch coupler) (Fig. 4.2b), which can be operated by a switch in the tractor cab. The generator is mounted on the SAS body, because removability from the tractor is considered as important. The spectrometers were changed to C10083CAH (320–1100 nm, 0.3 nm/interval) and C9406GC (900–1700 nm, 1.6 nm/interval) produced by the Hamamatsu Photonics Co., Ltd. The halogen lamp was changed to JCR15V150W/AL produced by the Fuji Lamp Co., Ltd. The automatic retreat function of the soil penetration part was excluded, and it was changed to using a share

pin to prevent the soil penetration part from breakage. System updates and maintenance can be performed remotely via a communication line.

(3) SAS2600

SAS2600 (weight: 750 kg) was designed for a Japan's research project entitled with *Research and Development for Increased Woody Biomass Production through Genome Breeding and High Efficiency Forestry Operations* which was adopted in 2013 under the Development of Efficient Elemental Technologies for Biofuel Production funded by the New Energy and Industrial Technology Development Organization (NEDO). The prototype was produced with specification determined for Brazil's woodlot.

The system configuration is the same as SAS2500, and improvements and changes were made to reinforce the frame strength to approximately 1.2 times in deflection amount of SAS2500 (steel thickness 4.5–6 mm) and were equipped with a beam knife, as a countermeasure for eucalyptus plant's residual and hard soil. The DGPS receiver was changed to the model SPS351 (Nikon Trimble Co., Ltd.)

(4) SAS3000

SAS3000 was produced under a research project entitled the special scheme project on regional developing strategy (project ID14526726 and 16781474) by the NARO Bio-oriented Technology Research Advancement Institution (Fig. 4.3). The system configuration is the same as SAS2500, and improvements and changes were made by permanently installing a touch panel in the tractor cab, which enables one operation for the SAS setting. The observation speed is 0.28–1.68 m/s, and the weight was reduced to 510 kg. The DGPS receiver was changed to model SPS351 (Nikon Trimble Co., Ltd.).

4.1.4 *Analysis of Calibration Model for Multiple Soil Properties*

(1) Absorption Wavelength and Regression Coefficient Estimation

The moisture content (MC), humic acid (total carbon (TC), total nitrogen (TN)), soil organic matter (SOM), clay (CL, 1:1 type and 1:2 type), available silicate (SiO), and free iron oxide (Fe) have the absorption wavelength in the analysis wavelength range. Therefore, the regression coefficients can be estimated, and the negative peak waveform of the regression coefficient matches the absorption wavelength for each property (in the case of second-order differential absorbance).

Soil properties with no absorption wavelength within the analytical wavelength range (available phosphorus (P-a), exchangeable potassium (K), exchangeable calcium (Ca), exchangeable magnesium (Mg), exchangeable sodium (Na), ammonia nitrogen (N-a), nitrate nitrogen (N-n), hot-water-extractable nitrogen (N-h), hot water soluble boron (B), soluble zinc (Zn), soluble copper (Cu), easily reducible manganese (Mn), exchange acidity (y1), phosphate absorption coefficient (PAC),

pH, EC, CEC, 2:1-type minerals CL and sand (S), silt (SL), dry density (ρd), cal-
cium/magnesia ratio (Ca/Mg), magnesium/potassium ratio (Mg/K), base saturation
percentage (BSP), calcium saturation percentage (CSP), sodium ratio (Na-r), and
carbon-nitrogen (C/N) ratio) correlated with the analysis values of organic, inor-
ganic substances whose absorbance wavelength has been confirmed within the ana-
lytical wavelength range (Matsunaga and Uwasawa 1992b; Clark et al. 1987;
Umeda et al. 2001; Zornoza et al. 2008). In the case of raw soil, the regression
coefficients can be estimated due to the spectra variation caused by the hydration
phenomenon of inorganic ion component and binding with organic molecules. The
negative peak waveform of the regression coefficient was consistent with the absorp-
tion wavelength of the correlated properties.

The possibility of regression coefficient estimation can be evaluated from the
correlation between soil analysis values, which is based on the evaluation and clas-
sification using correlation coefficient (R). The classification methods include
Pearson product-moment correlation (interval and ratio scale data) and Spearman's
rank correlation (rank scale data). In addition, Pearson product-moment correlation
was adopted (Table 4.3).

To confirm the correlation and reliability of regression coefficients, it was con-
firmed that the obtained regression coefficient for each property used the absorption
wavelength or absorption wavelength band, by confirming that the negative absorp-
tion peak of each regression coefficient for each property from 1 to selected F
(PLSR factor) value was in agreement with the absorption wavelength or exists in
the absorption wavelength band. When the fluctuation of the spectra is large due to
the hydration phenomenon of the inorganic ion and binding with organic molecules,
it may not completely match due to the wave number shift.

(2) Evaluation/Classification   Methods   of   Regression   Coefficient   and
    Prediction Values

The evaluation indexes of regression coefficient estimation accuracy of soil are
R^2, RPD, range error ratio (RER), and evaluation index (EI). There are several
guidelines for the evaluation and classification based on R^2 and RPD. Here, guide-
lines for evaluation/classification without over-/under-evaluation are presented.

Table 4.3 Evaluation and classification of the correlation between soil analysis values using
correlation coefficient

Evaluation	Classification				
Full correlation			$|R|$	$=$	1
Highly correlated	0.7	$<$	$|R|$	$<$	1
Correlated	0.4	$<$	$|R|$	$\leqq$	0.7
Low correlation	0.2	$<$	$|R|$	$\leqq$	0.4
Almost no correlation	0	$<$	$|R|$	$\leqq$	0.2
No correlation	0	$=$	$|R|$		

The possibility of estimation of regression coefficient for properties whose absorption wavelength is not confirmed in the analysis wavelength region is based on the correlation between soil analysis values. Therefore, in the correlation coefficient classification method shown in Table 4.4, the R range from 0.7 to 1.0, which is "highly correlated," is divided into four threshold values "0.95, 0.9, 0.8, and 0.7." Squaring each of the value, R then becomes "0.90, 0.81, 0.64, and 0.49," and R^2 threshold values are obtained. It has been decided to classify R^2 using these threshold values. This classification method is consistent with ranks "B, C, and D" of Malley et al. (2004). Ranks "A and D" are consistent with Kuang et al. (2012). Therefore, it is an intermediate classification between the two methods. The RPD used middle of Kuang et al. (2012), RER used Malley et al. (2004), and EI used Mizuno et al. (1987).

The evaluation and classification method using the combination of R^2 and RPD is to evaluate the availability of the estimated regression coefficients and the prediction values. Further, the combinations of R^2 and RER and R^2 and EI are to evaluate whether the estimated regression coefficients are composed of an enough range. In each combination, if they did not belong to the same rank, lower rank was selected.

(3) An Example of Regression Coefficient Estimation (Paddy Field)

(i) Test Fields

The test fields were agricultural production corporation Denpata (sandy clay loam, S = 64.6%, SL = 14.6%, CL = 20.8%) and Yokota farm (light clay, S = 52.8%, SL = 17.3). The test devices were SAS2500 and SAS3000. The sampling interval was 3 s. The observation speed was 0.28 m/s. The observation depth was 0.10 m determined by the grower. As the soil characteristics, the ratio of CL in Yokota farm was high, and the retainability of fertilizer was high. An overview of the analysis database is summarized in Table 4.5. The data collection for the test field was at 5 times in 3 years, from 48 fields. The total number of the collected data was 552, but 406 data for pH and EC, exchangeable sodium, and sodium ratio and 364 data for S, SL, CL, available silicate, and free iron oxide were used to estimate regression coefficient.

Table 4.4 Evaluation and classification methods using R^2 with RPD, RER, and EI

Evaluation	R^2	RPD	RER	EI (%)	Rank
Excellent	0.90<	3.0<	20<	≤12.4	A
Good	0.81-0.90	2.5-3.0	15-20	12.5-24.9	B
Approximate quantitative prediction	0.64-0.81	2.0-2.4	10-15	25.0-37.4	C
Distinguish between high and low	0.49-0.64	1.5-1.9	8-10	37.5-49.9	D
Not usable	<0.49	<1.5	<8	50.0≦	E

※Rank is classified into A–E, as "regression coefficient, prediction value": A, excellent; B, good; C, approximate quantitative prediction; D, distinguish between high and low; E, not usable

Table 4.5 Database for analysis

Implementation date	Location	Test field	Equipment	Number of test fields	Field size (ha)	Number of data
2013.12.06	Fukushima Prefecture	Denpata Farm	SAS2500	4	1.0	188
2014.09.23~24			SAS2500	4	1.2	118
2014.11.13~15	Ibaraki Prefecture	Yokota Farm	SAS2500	5	6.4	100
2015.10.25~27			SAS3000	10	10	120
2015.12.15~17			SAS3000	25	24	26
Total				48	42	552

(ii) Determination of Validation Method

The requirements to divide the dataset into calibration set and prediction set are pluralities of the same data that exist, with an unbiased frequency distribution, while a rectangular-shape distribution is expected (Akitomo and Shimamura 1998). The obtained distribution in this study was close to normal distribution, and the shape with two peaks also existed. The requirements of dividing for calibration set and prediction set were not satisfied. Therefore, full cross-validation was applied.

(iii) Correlation Between Analysis Values

For properties whose absorption wavelength was not confirmed in the analysis wavelength range, correlation coefficients between soil analysis values were obtained, and the correlations were summarized in Table 4.6 according to the classification in Table 4.3. Positive correlations are shown in black, and negative correlations are shown in red. "Correlation" (gray highlight) or "high correlation" (yellow highlight) with properties that have absorption wavelength in the analysis wavelength range are counted as direct correlation. "Correlation" and "high correlation" were counted as indirect correlation between the properties whose absorption wavelength has not been confirmed in the analysis wavelength range. Properties with many direct correlations have strong collinearity between analysis values of properties that have absorption wavelength in the analysis range, and the possibility to estimate regression coefficients is also high. Indirect correlations are less collinear than direct correlations, and the possibility to estimate regression coefficient is less than the direction correlation. But the possibility varies depending on the total number of correlations and the concentration distribution of the analysis values.

Twenty-two properties whose absorption wavelength has not been confirmed in the analysis wavelength range had correlation with eight properties that have an absorption wavelength (blue font in Table 4.6). The properties that have no direct correlation were base saturation, lime saturation, sodium ratio, and soluble zinc. The property that has no indirect correlation was soluble zinc. Therefore, it was 33 properties that could explain that the regression coefficients could be estimated by the correlation between the analysis values. The estimation of regression coefficient of soluble zinc could not be explained by the correlation with the analysis values.

Table 4.6 Correlation coefficient between analysis values

項目	N-a	N-h	N-n	N-t	P-a	SiO	K	Ca	Mg	Na	Fe	Cu	Zn	B	Mn	EC	CEC	Ca/Mg	Mg/K	BSP	CSP	ESP	HR	SOM	C-1	C/N	pH	yl	PAC	MC	pd	S	SL	CL
N-a	1.000																																	
N-h	-0.014	1.000																																
N-n	0.331	0.300	1.000																															
N-t	0.171	0.514	0.514	1.000																														
P-a	-0.583	-0.112	-0.579	-0.437	1.000																													
SiO	0.469	0.149	0.141	0.338	-0.298	1.000																												
K	0.572	0.196	0.354	0.402	-0.701	0.426	1.000																											
Ca	0.537	0.389	0.564	0.688	-0.770	0.283	0.742	1.000																										
Mg	0.666	0.155	0.491	0.444	-0.821	0.322	0.834	0.888	1.000																									
Na	0.550	0.260	0.411	0.449	-0.819	0.440	0.619	0.635	0.738	1.000																								
Fe	0.633	0.297	0.448	0.550	-0.765	0.457	0.742	0.832	0.829	0.690	1.000																							
Cu	0.141	0.343	0.289	0.545	-0.578	0.289	0.293	0.498	0.360	0.441	0.404	1.000																						
Zn	-0.029	0.007	-0.018	-0.005	-0.115	-0.085	0.022	0.077	0.027	0.068	0.096	0.184	1.000																					
B	0.191	0.563	0.482	0.499	-0.428	0.231	0.273	0.564	0.304	0.374	0.433	0.606	0.114	1.000																				
Mn	0.561	0.140	0.499	0.490	-0.879	0.493	0.692	0.635	0.817	0.793	0.788	0.680	0.025	0.404	1.000																			
EC	-0.271	0.057	-0.206	-0.000	0.135	-0.602	-0.078	-0.019	-0.104	-0.349	-0.417	-0.202	0.045	0.014	-0.064	1.000																		
CEC	0.446	0.457	0.683	0.714	-0.805	0.317	0.659	0.916	0.916	0.712	0.788	0.663	0.060	0.652	0.826	-0.126	1.000																	
Ca/Mg	-0.573	0.075	-0.361	-0.091	0.732	-0.191	-0.709	-0.517	-0.799	-0.676	-0.551	-0.271	-0.016	-0.064	-0.654	0.484	-0.540	1.000																
Mg/K	0.485	0.109	0.504	0.375	-0.700	0.012	0.319	0.692	0.752	0.575	0.525	0.385	0.132	0.302	0.667	-0.058	0.709	-0.613	1.000															
BSP	0.370	-0.205	-0.284	-0.144	-0.002	0.343	0.241	0.334	0.120	0.214	0.161	0.084	0.200	0.117	-0.115	0.439	-0.230	-0.220	0.117	1.000														
CSP	-0.260	-0.322	-0.260	-0.286	0.131	-0.055	0.064	0.031	0.073	0.120	0.073	-0.329	0.100	-0.230	-0.066	0.443	-0.294	-0.203	0.169	0.913	1.000													
ESP	0.487	-0.246	-0.069	-0.241	-0.395	0.159	0.276	-0.011	0.273	0.619	0.091	-0.041	0.053	-0.188	0.297	-0.613	-0.049	-0.527	0.168	0.387	0.162	1.000												
HR	0.278	0.664	0.563	0.968	-0.573	0.290	0.508	0.814	0.600	0.498	0.649	0.600	0.018	0.706	0.600	-0.034	0.874	-0.229	0.515	-0.181	-0.233	-0.223	1.000											
SOM	0.525	0.517	0.611	0.850	-0.717	0.467	0.642	0.870	0.750	0.626	0.810	0.625	0.031	0.684	0.780	-0.100	0.909	-0.428	0.608	-0.069	-0.203	-0.093	0.909	1.000										
C-1	0.278	0.664	0.563	0.968	-0.573	0.290	0.508	0.814	0.600	0.498	0.649	0.563	0.018	0.706	0.600	-0.034	0.874	-0.229	0.515	-0.181	-0.233	-0.223	1.000	0.795	1.000									
C/N	0.410	-0.085	0.139	0.142	-0.463	0.426	0.326	0.391	0.455	0.458	0.445	0.293	0.132	0.318	0.517	-0.213	0.558	-0.254	0.393	0.073	-0.010	0.460	0.205	0.267	0.205	1.000								
pH	0.353	0.177	0.403	0.288	-0.499	-0.101	0.424	0.425	0.455	0.310	0.439	0.374	-0.003	0.285	0.417	-0.074	0.487	-0.465	0.353	-0.078	-0.255	0.017	0.387	0.458	0.387	0.537	1.000							
yl	0.664	0.304	0.490	0.613	-0.718	0.498	0.793	0.873	0.855	0.599	0.887	0.445	0.023	0.580	0.785	0.044	0.799	-0.547	0.563	0.241	-0.246	-0.087	0.718	0.864	0.718	0.778	-0.193	1.000						
PAC	-0.055	0.327	0.139	0.323	-0.344	0.323	0.364	0.524	0.314	0.485	0.462	0.433	0.035	0.580	0.388	0.192	0.613	-0.088	0.236	-0.240	-0.246	-0.087	0.775	0.670	0.775	0.385	0.242	0.468	1.000					
MC	-0.268	-0.572	-0.218	-0.572	-0.801	-0.416	-0.607	-0.606	-0.588	-0.694	-0.613	-0.015	-0.109	-0.381	-0.631	0.010	-0.826	0.404	-0.440	-0.136	-0.153	-0.516	-0.823	-0.837	-0.823	-0.621	0.103	-0.410	-0.708	1.000				
pd	0.320	0.294	0.005	0.279	-0.581	0.047	0.279	0.524	0.314	0.130	0.462	0.433	0.013	0.208	0.164	-0.848	0.183	0.183	-0.136	0.026	0.309	0.113	0.130	0.390	0.130	-0.394	-0.109	-0.362	-0.720	-0.751	1.000			
S	0.413	0.294	0.005	0.362	-0.576	0.522	0.287	0.175	0.130	0.125	0.286	0.093	-0.043	0.208	0.164	-0.734	0.149	0.111	-0.153	-0.027	0.009	0.113	0.294	0.390	0.294	0.036	0.369	-0.362	-0.452	0.295	0.630	1.000		
SL	0.005	0.047	0.362	0.279	-0.474	0.522	0.287	0.175	0.130	0.125	0.286	0.093	-0.043	0.208	0.164	-0.153	0.149	0.111	-0.153	-0.027	0.009	0.113	0.294	0.390	0.294	0.036	0.358	-0.088	-0.751	-0.362	-0.362	-0.809	1.000	
CL	0.539	0.335	0.401	0.581	-0.474	0.457	0.631	0.680	0.669	0.511	0.755	0.350	0.017	0.414	0.613	-0.713	0.676	-0.380	0.342	0.045	-0.049	-0.093	0.627	0.769	0.627	0.582	0.415	0.404	0.775	0.450	-0.670	-0.864	0.403	1.000
D.C.[*1]	4	6	5	6	3	3	7	7	6	6	7	6	0	7	7	2	6	2	4	2	2	0	6	6	6	6	3	3	6	6	8	8	2	7
I.C.[*2]	14	4	13	15	17	9	13	17	16	16	20	10	0	10	17	5	17	14	16	2	2	5	16	19	16	16	6	11	18	9	17	10	4	16
Total	18	10	18	21	23	12	20	24	22	24	27	16	0	17	24	5	23	16	16	2	2	5	22	22	22	22	6	13	26	15	25	25	4	23

*1; Direct correlation; Correlation with properties whose absorption wavelength exist in the analysis wavelength range, and the value is more than "correlated"

*2; Indirect correlation; Correlation with properties whose absorption wavelength do not exist in the analysis wavelength range, and the value is more than "correlated"

Grey highlight; |R|>0.4 「Correlated」,   Yellow highlight; |R|>0.7 「Highly correlated」

[a]**Direct correlation:Correlation with properties whose absorption wavelength exist in the analysis wavelength range, and the value is more than "correlated"**

[b]Indirect correlation:Correlation with properties whose absorption wavelength do not exist in the analysis wavelength range, and the value is more than "correlated"

Grey highlight; |R|>0.4 「Correlated」, Yellow highlight; |R|>0.7 「Highly correlated」

(iv) PLSR Results

According to the absorbance in the analysis database (Fig. 4.4a), the spectra change is large at 350–400 nm, and it has a peak of positive waveform at 1400 nm and baseline shift. According to second-derivative absorbance of the S-G (Savitzky-Golay) method with smoothing point (SP) = 41 (Fig. 4.4b), which has the highest smoothing effect, four data were confirmed as outliers which had negative peaks at 600–700 nm. But the absorption wavelength of humic acid is 620 nm. According to the frequency distribution of humic acid shown in Fig. 4.4c, since about 14% of the analysis values were higher than others, they were not excluded.

Table 4.7 and 4.8 summarizes the estimation results of regression coefficients obtained through repeatedly running PLSR algorithm by excluding data with the largest prediction residual (outlier) at each run. Table 4.7 shows the statistical values of each property, and Table 4.8 shows the accuracy, evaluation, and classification of each regression coefficient. The accuracy of each property satisfies the condition of $R^2 > 0.9$ and $F \leq 10$. In addition, since the evaluation/classification of calibration was $Rank_{RPD} = A$, the reliability of regression coefficient was obtained. The $Rank_{RPD} = C$ was obtained for exchangeable magnesia, S, and CL in evaluation/classification of validation. To improve the reliability of the prediction value to "$Rank_{RPD}=B$," it is necessary to reanalyze by adding data.

To evaluate the range of database that constitutes the regression coefficient, the classification using RER and EI can be considered. Since RER is more strict evaluation of the 34 properties, they were evaluated by RER. The RER results were $Rank_{cal}=C$ for available phosphorus, exchangeable potassium, exchangeable sodium, free iron oxide, soluble zinc, easily reducible manganese, EC, CEC, lime/magnesia ratio, magnesia/potassium ratio, soil organic matter, C/N, pH, exchange acidity, and ρd. It is necessary to add data in the range not possessed and re-analyze.

(v) Soil Analysis and Regression Coefficient

To show the detail of the database that constitutes the regression coefficients for each estimated property, scatter plots of analysis values and prediction values and regression coefficients are summarized, and several examples are shown in Fig. 4.5. The reference range of soil analysis (Agricultural Product Chemical Research Laboratory 2001; Yamazaki 2008) was described (Table 4.9). However, the reference range differs according to location, crop, and variety (Ministry of Agriculture Forestry and Fisheries 2008b, 2016a). For exchangeable calcium, the analysis value corresponding to the lime saturation of 40–60% is within the appropriate range and can be calculated from Eq. (4.1):
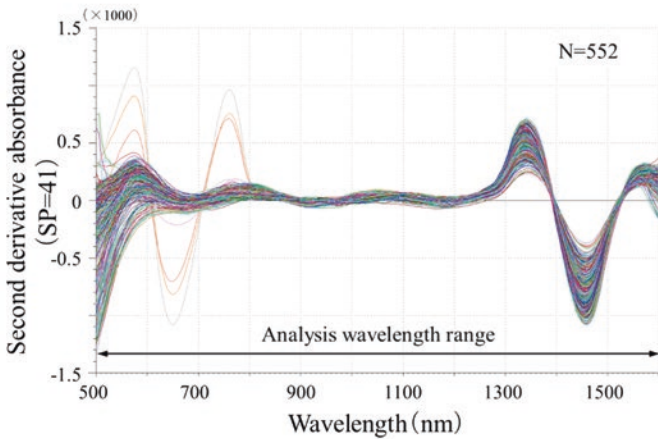
$$Calcium\,saturation\,percentage = Ca_{me} \, / \, CEC \times 100 \qquad (4.1)$$
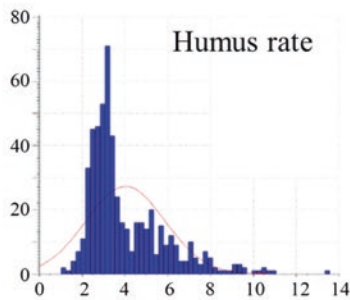
$$Ca_{me} = Ca \, / \, 28.04$$

The reference range for CEC and humic acid differs with soil type. The reference range of phosphate absorption coefficient is for dry field farming in Hokkaido, and the estimated phosphate utilization rate for crops is less than 700 (20–30%),
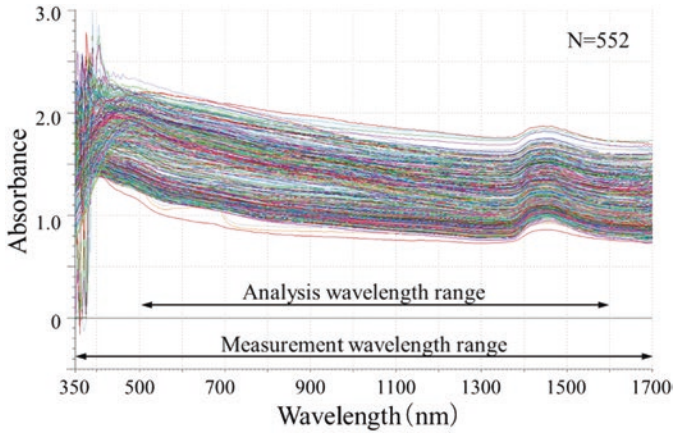
(a) Absorbance of the analysis database

(b) Second derivative absorbance of the analysis database

(c) Scatter plots of humus rate

Fig. 4.4 An example of PLS regression coefficient estimation (**a**) Absorbance of the analysis database (**b**) Second-derivative absorbance of the analysis database (**c**) Scatter plots of humus rate

Table 4.7 Thirty-four properties' regression coefficient estimation accuracy and evaluation/classification results (statistics)

Property	Unit	N_{Cal}∣N	Range				S.D.	SDP		RMSE	
			Min	Max	Min_{Cal}	Max_{Cal}		Cal	Val	Cal	Val
N-a	mg/100 g	349∣552	0.26	8.30	0.30	2.99	0.47	0.148	0.182	0.148	0.182
N-h	mg/100 g	287∣552	2.18	14.7	2.18	6.91	0.74	0.234	0.250	0.234	0.250
N-n	mg/100 g	292∣552	0.00	3.85	0.00	0.93	0.19	0.059	0.062	0.059	0.062
N-t	%	338∣552	0.07	0.58	0.07	0.26	0.03	0.009	0.010	0.009	0.010
P-a	mg/100 g	538∣552	1.54	34.4	1.54	34.3	9.94	3.096	3.301	3.094	3.298
SiO	mg/100 g	225∣364	12.5	103	14.4	73.5	9.88	3.052	4.255	3.045	4.264
K	mg/100 g	462∣552	1.69	52.6	5.38	28.4	5.22	1.645	1.797	1.643	1.795
Ca	mg/100 g	538∣552	44.3	668	44.3	614	112	35.22	40.37	35.18	40.33
Mg	mg/100 g	535∣552	3.52	180	3.52	148.0	29.9	9.424	12.37	9.415	12.36
Na	mg/100 g	270∣364	0.58	26.3	0.58	15.0	3.79	1.192	1.275	1.189	1.273
Fe	mg/100 g	320∣364	0.04	3.10	0.22	2.68	0.68	0.215	0.244	0.215	0.244
Cu	ppm	335∣552	0.81	15.0	3.24	10.9	1.33	0.420	0.489	0.419	0.488
Zn	ppm	272∣552	2.56	62.5	3.01	5.56	0.57	0.179	0.211	0.178	0.211
B	ppm	351∣552	0.41	1.70	0.41	1.37	0.14	0.045	0.054	0.045	0.054
Mn	ppm	526∣552	3.59	266	3.59	218	63.6	20.07	22.71	20.05	22.69
EC	mS/cm	363∣406	0.01	0.09	0.01	0.06	0.02	0.005	0.006	0.005	0.006
CEC	me/100 g	551∣552	7.18	42.3	7.18	42.3	8.96	2.833	3.056	2.831	3.053
Ca/Mg	E.R	459∣552	1.91	9.05	1.91	6.45	1.24	0.391	0.408	0.391	0.407
Mg/K	E.R	387∣552	2.95	20.5	3.62	11.8	1.85	0.578	0.657	0.577	0.656
BSP	%	358∣552	19.9	114	43.1	102	9.37	2.960	3.322	2.956	3.318
CSP	%	315∣552	17.6	84.9	32.7	68.9	5.90	1.865	2.216	1.862	2.213
ESP	%	212∣364	0.18	5.38	0.45	2.41	0.35	0.119	0.137	0.110	0.128
HR	%	505∣552	1.02	13.6	1.02	8.82	1.46	0.459	0.570	0.459	0.570
SOM	%	502∣552	4.61	19.0	4.74	15.3	2.43	0.766	0.838	0.765	0.837
C-t	%	485∣552	0.59	7.88	0.59	4.78	0.77	0.237	0.287	0.237	0.286
C/N	–	551∣552	6.73	16.7	9.00	16.7	1.75	0.547	0.621	0.546	0.621
pH	–	288∣406	5.61	6.76	5.74	6.49	0.17	0.043	0.048	0.054	0.067
y1	–	277∣552	0.06	2.50	0.19	1.00	0.18	0.058	0.065	0.057	0.065
PAC	–	537∣552	8.00	1518	8.00	1509	297	89.37	103.7	89.29	103.6
MC	–	288∣552	28.3	115	30.7	53.3	4.17	1.314	1.424	1.312	1.422
DD	g/cm³	389∣552	0.61	1.03	0.76	1.00	0.06	0.018	0.021	0.018	0.021
S	%	250∣364	18.4	75.5	29.5	72.2	7.78	2.586	3.659	2.047	3.014
SL	%	240∣364	5.68	47.8	8.44	30.5	3.84	1.201	1.551	1.198	1.548
CL	%	290∣364	13.2	51.1	18.2	43.2	4.96	1.562	2.259	1.529	2.144

E.R equivalence ratio

700–1500 (15–20%), and 1500–2000 (10%–15%) and more than 2000 (6–10%). The reliable range of the prediction values using the regression coefficients of 34 properties is the range of the analysis values in the scatter plots. For hot water extractable nitrogen, the range was 2.2–6.9 mg/100 g, including the reference range. But it cannot be used in soil analysis for high concentration data because it is not

Table 4.8 Thirty-four properties' regression coefficient estimation accuracy and evaluation/classification results (accuracy/evaluation/classification)

Property	SP	F	R^2 Cal	R^2 Val	RPD Cal	RPD Val	Rank$_{RPD}$ Cal	Rank$_{RPD}$ Val	RER Cal	RER Val	Rank$_{RER}$ Cal	Rank$_{RER}$ Val	EI Cal	EI Val	Rank$_{EI}$ Cal	Rank$_{EI}$ Val
N-a	7	7	0.90	0.85	3.17	2.57	A	B	18.2	14.7	B	C	11.0	13.6	A	B
N-h	17	6	0.90	0.89	3.17	2.97	A	B	20.2	18.9	A	B	9.9	10.6	A	A
N-n	13	4	0.90	0.89	3.17	3.00	A	B	15.8	14.9	B	B	12.7	13.4	B	B
N-t	7	6	0.90	0.87	3.18	2.76	A	B	20.5	17.8	A	B	9.8	11.3	A	A
P-a	7	5	0.90	0.89	3.21	3.01	A	B	10.6	9.93	C	C	18.9	20.2	B	B
SiO	7	8	0.90	0.82	3.25	2.32	A	B	19.4	13.9	B	C	10.3	14.4	A	B
K	15	8	0.90	0.88	3.18	2.91	A	B	14.0	12.8	C	C	14.3	15.6	B	B
Ca	17	9	0.90	0.87	3.18	2.77	A	B	16.2	14.1	B	C	12.4	14.2	A	B
Mg	3	8	0.90	0.83	3.18	2.42	A	C	15.4	11.7	B	C	13.0	17.1	B	B
Na	21	6	0.90	0.89	3.18	2.97	A	B	12.2	11.4	C	C	16.5	17.6	B	B
Fe	9	5	0.90	0.87	3.18	2.81	A	B	11.5	10.1	C	C	17.5	19.8	B	B
Cu	3	5	0.90	0.87	3.18	2.73	A	B	18.2	15.7	B	B	11.0	12.8	A	B
Zn	15	9	0.90	0.86	3.19	2.70	A	B	14.3	12.1	C	C	14.1	16.6	B	B
B	7	7	0.90	0.86	3.17	2.65	A	B	21.4	17.9	A	B	9.34	11.2	A	A
Mn	7	5	0.90	0.87	3.17	2.80	A	B	10.7	9.45	C	C	18.7	21.2	B	B
EC	7	5	0.90	0.88	3.17	2.85	A	B	10.6	9.60	C	D	18.8	20.9	B	B
CEC	21	8	0.90	0.88	3.17	2.94	A	B	12.4	11.5	C	C	16.1	17.4	B	B
Ca/Mg	15	6	0.90	0.89	3.17	3.04	A	B	11.6	11.1	C	C	17.2	18.0	B	B
Mg/K	11	8	0.90	0.87	3.21	2.82	A	B	14.1	12.4	C	C	14.2	16.2	B	B
BSP	15	9	0.90	0.88	3.17	2.83	A	B	20.0	17.8	A	B	10.0	11.2	A	A
CSP	9	8	0.90	0.86	3.17	2.67	A	B	19.5	16.4	B	B	10.3	12.2	A	A
ESP	15	7	0.90	0.87	3.18	2.74	A	B	17.8	15.3	B	B	12.1	14.0	A	B
HR	7	8	0.90	0.85	3.18	2.56	A	B	17.0	13.7	B	C	11.8	14.6	A	B
SOM	9	5	0.90	0.88	3.18	2.90	A	B	13.9	12.7	C	C	14.4	15.8	B	B
C-t	7	7	0.91	0.86	3.25	2.69	A	B	17.7	14.6	B	C	11.3	13.7	A	B
C/N	9	6	0.90	0.88	3.21	2.83	A	B	14.1	12.4	C	C	14.2	16.2	B	B
pH	9	8	0.90	0.85	3.17	2.58	A	B	13.9	11.3	C	C	11.4	12.8	A	B
y1	7	4	0.90	0.87	3.20	2.84	A	B	14.1	12.5	C	C	14.2	16.0	B	B
PAC	15	10	0.91	0.88	3.32	2.86	A	B	16.8	14.5	B	C	11.9	13.8	A	B
MC	9	4	0.90	0.88	3.17	2.93	A	B	17.2	15.8	B	B	11.7	12.6	A	B
DD	7	6	0.90	0.87	3.18	2.76	A	B	13.3	11.6	C	C	15.0	17.3	B	B
S	9	10	0.93	0.85	3.80	2.58	A	B	20.9	14.2	A	C	12.1	17.1	A	B
SL	11	9	0.90	0.84	3.21	2.48	A	B	18.4	14.2	B	C	10.9	14.1	A	B
CL	9	10	0.90	0.81	3.25	2.31	A	C	16.3	11.7	B	C	12.5	18.1	B	B

included in the regression coefficient database. The available phosphorus database included the reference range of 10–30 mg/100 g, so it can be used in the soil analysis. However, since data at 10–20 mg/100 g is missing, additional data and reanalysis in this range are required. Exchangeable magnesia, exchangeable sodium, and C/N also need reanalysis with intermediate data added. The ideal database of
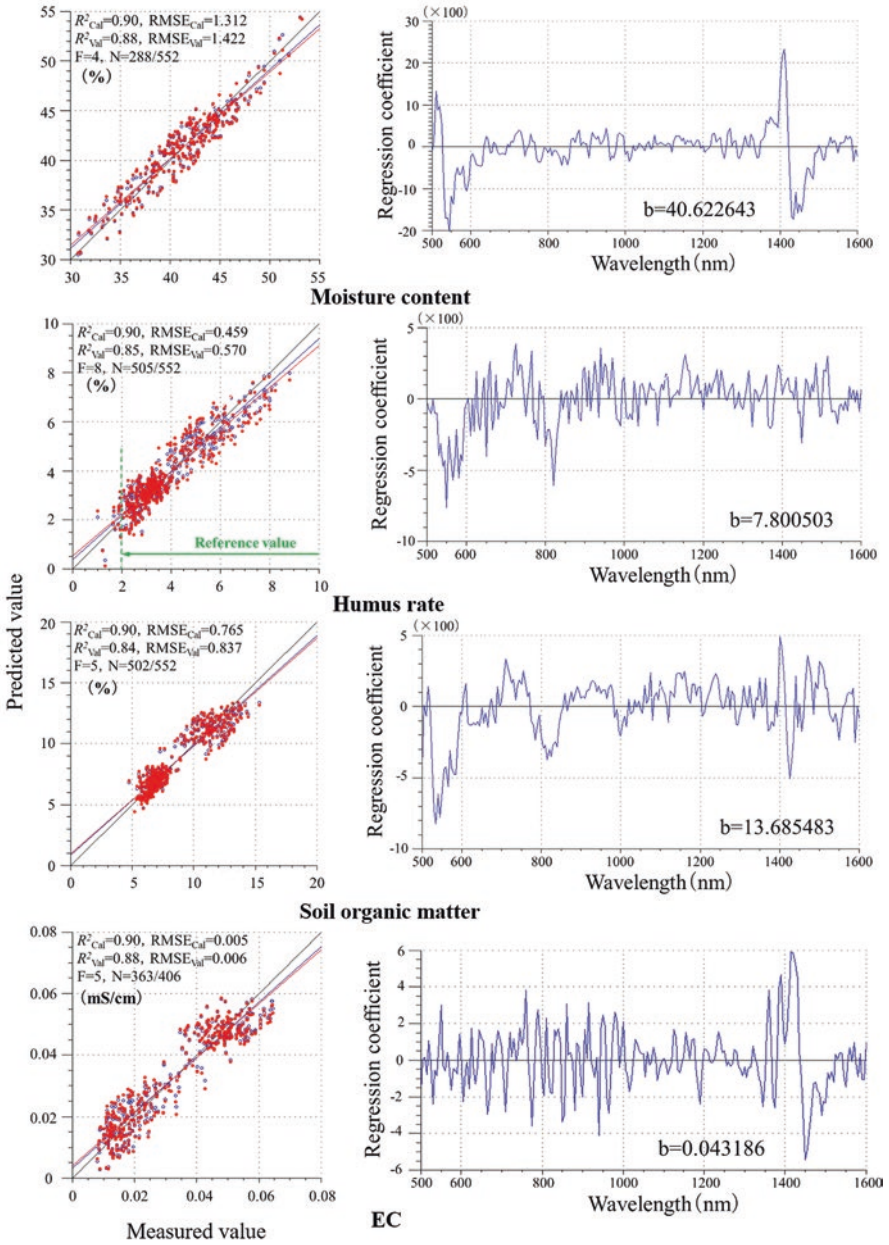
Fig. 4.5 Scatter plots of analysis and prediction values and regression coefficient

Table 4.9 Reference value of soil analysis

Property	Unit	Reference value			Property	Unit	Reference value		
pH	–	5.5	~	6.5	PAC	–	–	~	–
P-a	mg/100 g	10	~	30	CEC	me/100g	20	~	30
K	mg/100 g	15	~	30	HR	%	2	~	
Mg	mg/100 g	25	~	45	EC	mS/cm	0.4	~	0.6
Mg/K	E.R.	2	~		y1	–	–	~	–
Ca/Mg	E.R.		~	6	SOM	%	3	~	
Ca	mg/100 g	200	~	300	C-t	%	–	~	–
CSP	%	40	~	60	C/N	–	15	~	30
BSP	%	60	~	80	SiO	mg/100g	15	~	30
Cu	ppm	0.5	~	8.0	Fe	%	0.8	~	4.0
Zn	ppm	2	~	40	Na	mg/100g		~	15
Mn	ppm	50	~	500	ESP	%		~	20
B	ppm	0.5	~	1.0	MC	%	–	~	–
N-h	mg/100 g	5	~	7	DD	g/cm3	–	~	–
N-t	%	–	~	–	S	%	–	~	–
N-n	mg/100 g	–	~	–	SL	%	–	~	–
N-a	mg/100 g	–	~	–	CL	%	–	~	–

analysis and prediction values for the purpose of soil analysis were CEC, exchangeable calcium, base saturation, lime saturation, and free iron oxide.

(vi) Regression Coefficient and Absorption Wavelength

As the regression coefficient of each property has been applied with second derivative, the negative coefficient is almost the same with the peak waveform of the absorption wavelength. In soil water content whose absorption wavelength exists in the analysis wavelength region, the negative peak matches the water's absorption wavelength (1450 nm) (Fig. 4.5). In addition, the negative peak near 550 nm coincides with the green wavelength band, which is the complementary color of red, and it is necessary to consider the analysis wavelength region because of the effect of soil color. Furthermore, the regression coefficient waveform of soil water content has almost the same shape with the second-derivative absorbance spectra. Moreover, the regression coefficients in 600–1350 nm, which are not directly related to the absorption wavelength, seem to eliminate the baseline noise of the second-derivative absorbance. The negative peaks of soil organic matter, humus rate, total carbon, and total nitrogen were consistent with the absorption wavelength of humic acid (570 nm, 620 nm, 1100–1600 nm). The negative peaks of available silicate coincided with the absorption wavelength (930 nm, 1000 nm), and negative peaks were also confirmed at 570 nm and 620 nm because of its correlation with the organic content. Two negative peaks were observed in free iron oxide absorption band (1380–1410 nm), and a large negative peak was observed at 530 nm in the Fe^{3+} absorption band (500–800 nm). Although the absorption wavelength of CL is 1400 nm, no negative peak was observed in the regression coefficient. This is because when transforming to absorbance, 1400 nm was the conversion point

between the positive and negative peaks before and after 1400 nm, that is, zero. Since CL is composed of elements such as silicon and iron, multiple negative peaks of the regression coefficient were confirmed in the absorption wavelength of silicic acid and free iron oxide. The correlations between the analysis values of CL and free iron oxide and available silicate were "high correlation" and "correlation." As examples of regression coefficient estimation based on correlation with properties whose absorption wavelength exists, ammonia nitrogen has no correlation with the analysis value of total nitrogen, but its correlation with organic content was confirmed. Hot water extractable nitrogen was highly correlated with total carbon, total nitrogen, and humus rate. Nitrate nitrogen was correlated with total nitrogen, total carbon, and humus rate. Negative peaks were observed in the absorption wavelength of humic acid in each property.

The obtained regression coefficient for each property is a local regression coefficient corresponding to the database that consists of the analysis value range of the 34 properties used in the regression coefficient estimation. Moreover, it cannot satisfy all soil conditions as general purpose regression coefficient.

4.2   Application of Tractor-Mounted Soil Analysis System in Precision Agriculture

4.2.1   Site-Specific Soil Mapping and Interpretation of Agricultural Fields

(1) Soil Observation Preparation/Data Collection/Analysis/Visualization Process

The items of SAS setting before soil observation are observation speed (0.28–1.68 m/s), sampling period of diffuse reflectance spectra (3–10 s, 1 s interval), and observation depth (0.10–0.30 m, 0.05 m interval). The data acquisition interval in the direction of measurement is determined by observation speed and sampling period. But the data acquisition interval may not match the calculated value according to the soil conditions. If the observation speed is not constant, the measurement area of diffuse reflectance spectra and the soil sampling interval will be different. So, it will not be changed during the operation. By adjusting the gauge wheel to the track of the tractor's rare wheel, extra pitching fluctuation was avoided. The observation depth is the distance from the contact surface of the gauge wheel to the soil measurement surface leveled with a flat plate. When changing the observing depth, the top link was adjusted to ensure the SAS body's frame horizontal. Setting the observation depth deeply increases the traction resistance, so the tractor's drive condition and the model selection are important. In order to avoid the influence of tractor pitching, the draft control and position control of the tractor's three-point link hitch were not functioned, while a free suspension system was adopted.

The observation setting items before soil observation are the determination of number of observation lines and the endpoints of field where the shape of the field

can be easily understood. The number of observation lines and the interval between the observation lines are determined according to the grower's purpose of use of the soil map. For example, in the case of using the soil map for pest control and fertilization by a boom sprayer with one wing of 12 m, the first observation line was determined at 12 m from the field edge, and the second and later were determined at 24 m intervals. A glass pole was set at the field end in the traveling direction to improve the visibility of straight traveling. In the case of one-plot management, the field was firstly divided into three parts, and the observation lines were around the middle of each part. If there was no request from the grower, the least common multiple of the working width of the working machine owned by the grower was used. The settings of the observation line that have been requested in the past were the harvesting width of yield combined, the spray width of boom sprayer and broadcaster, and the width of planting line of rice transplanter.

After the SAS's power was turned on, it was waited about 15 min to stabilize the output of the halogen lamp. Before observing the first line of each plot, SRS40 was installed to the calibration jig set (Fig. 4.6b) in the soil penetration part to obtain white reference and dark reference data.

The position of soil samples, which were the objective variables for estimating the regression coefficient, was firstly confirmed by the alarm from the sensor when collecting spectra data and then marked on the soil surface by a half-split chopstick, while the data number was confirmed from the touch panel monitor simultaneously with the spectra data collection. The area was excavated by a shovel where the chopstick was placed at a wider area than the spectra measured area but did not disturb the observation surface of SAS. The residues and gravel were then removed. After that, using a stainless steel scoop, the soil at a depth with several centimeters from the observation surface with about 0.3 m in width and the surrounding soil with the same depth of the observation surface were collected and packed into a sealable plastic bag with a zip (Asahi Kasei Home Products Co. Ltd., Ziplock® Double zipper). About 1 kg was placed in the plastic bag, and it was closed by confirming that the zip did not bite the soil particles while the air was sufficiently pushed out. On the plastic bag, the symbol with field name, observation line number, and diffuse reflectance spectra number was recorded.

Two sets of soil samples were prepared at each sampling position, one set was analyzed at the Tokyo University of Agriculture and Technology (TUAT) and the other set was analyzed at the Agricultural Product Chemical Research Laboratory
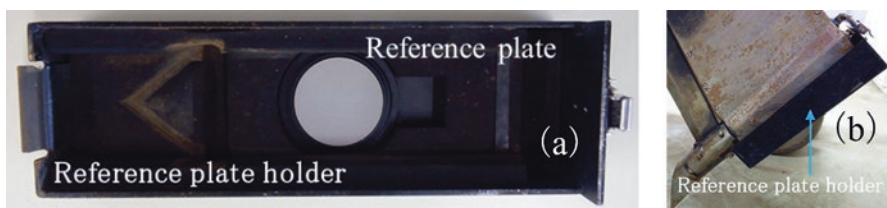
Fig. 4.6 Reference data acquisition method

(APCRL: Federation of Tokachi Agricultural Cooperative Association, Hokkaido, Japan). The soil samples were transported in refrigerators (0–10 °C) to restrain chemical composition change due to microbial activity. The soil samples sent to TUAT were stored in a refrigerator at 5 °C. Properties that could not be analyzed in TUAT were requested to be analyzed by APCRL. Properties that could not be analyzed in APCRL were analyzed by the Sumika Chemical Analysis Service, (SCAS) Ltd., using surplus dry soil samples used by APCRL. The analyzed values were not rounded by significant digits, but the display values of the weighing meter and measuring device and the total number of digits recorded on the recording medium of the device were used.

Once the soil analysis values were obtained, they were linked to the diffuse reflectance spectra, and a database for estimating the regression coefficients was constructed. The database was subjected to spectra preprocessing and PLSR analysis using multivariate analysis software (the Unscrambler Ver.9.8, CAMO Analytics AS). The prediction values were linked with position information and were visualized on a soil map. The visualization methods can be provided according to the grower's request, including interpolation map using the application software ArcMap of ArcGIS (ESRI Japan Co., Ltd.). The grid map divides a plot of field into grids with the mean, maximum, and minimum values shown in each grid. The dot map shows only the measurement point with dot of any size. When regression coefficient estimation is necessary, the black arrow and green arrow processes in Fig. 4.7 are necessary. When regression coefficient estimation is not required, blue arrow and green arrow processes are used to determine soil maps immediately after field observation.
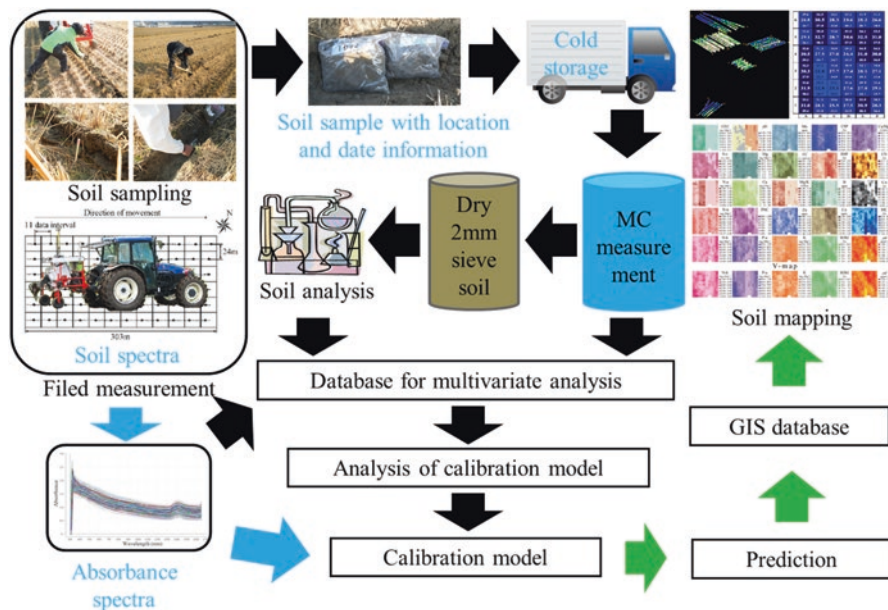
Fig. 4.7 Processes from field observation to soil mapping

(2) Soil Map

The soil map is defined as a spatial (or stratified) information at a certain date and time, with a high-resolution visualization of regional area, between fields or within field. Focusing on the plow layer, the soil map describes the information of soil physicochemical properties, biological properties, soil productivity (crop productivity such as yield), and soil fertility (conditions that support the root of crop and the ability of soil to supply the necessary amount of water and nutrients through the root according to the crop growth).

The purpose of creating a soil map is the management of local production area with group of crop cultivation fields or regional area and the soil management of grower-owned fields. In the management of local or regional area, the public infrastructure and environment necessary for crop cultivation and management are efficiently used, and profits are maximized by selecting crops and varieties. Higher efficiency in farm management requires the consolidation and accumulation of fields. The soil map is used as a source of information for decision-making and consensus building, such as improving workability by consolidating fields with similar fertility and reusing abandoned fields. The visualization method of one value per plot of field is the lowest resolution. The soil management of field owned by growers is based on the use of soil maps as a source of information on improving yield and quality as well as reducing production cost and environmental load through variable-rate work and crop or variety selection according to the variability between or within fields. The resolution of visualization varies according to the purpose of growers and their methods used in the farm management work.

The soil visualization information includes the terrain classification map, surface geological map, soil map, and groundwater map of the National Land Information Division, Ministry of Land, Infrastructure, Transport and Tourism, which were mainly used as sources of information for disaster countermeasures and building construction (Ministry of Land Infrastructure, Transport and Tourism 2018). Specialized for farmland use are soil profile map, fertility conservation soil map, and farmland soil map. The soil profile data is not used to directly control crop productivity, but the soil layer sequence that appears in the soil profile is the history of soil layer differentiation and shows whether the soil layer is going to maturity in the future. Therefore, it is an important information for reclamation of farmland and continuous design support on agricultural management. The problem is how to conduct soil survey up to 1 m soil depth and how to collect soil sample (Ministry of Agriculture Forestry and Fisheries 2016b). For the purpose of land use and farming guidance at municipal level, there are fertility conservation soil map data (Japan Soil Association) and farmland soil map data (Japan Soil Inventory, National Agriculture and Food Research Organization: NARO), which were compiled into database with physicochemical properties of the plow layer that cover the whole country. The farmland soil map is developed based on the data from the Fertilization Improvement Survey Project of the Ministry of Agriculture, Forestry and Fisheries, Fundamental Soil Survey for Fertility Conservation, Fundamental Soil-Environmental Survey, and Soil-Functional Monitoring Survey (about one point in

25 ha of soil profile survey in the farmland of Japan from 1953 to 2003) and the fertility conservation soil data. Seventeen properties were provided including thickness of plow layer (first layer), soil hardness (all soil layers hereinafter), bulk density, three phases (gas, liquid, solid), pF, water content, pH, exchange acidity, EC, total carbon, total nitrogen, base exchange capacity, exchangeable base, available phosphorus, available nitrogen, and suppliable silicic acid. The mean, median, standard deviation, and number of samples of each property were recorded for each of 60 soil groups. The scales of the farmland soil map are 1:200,000 and 1:50,000, and soil classification and soil temperature can also be viewed (Takada et al. 2013). The Agricultural Basic Law was enacted in 1961 which defined 0.3 ha as the standard plot (rice cultivation) in the field renovation project and was started in 1963 (Hirota 1999). The farmland soil map is composed of 1 data point per 83 plots (25 ha/0.3 ha). In addition, the cultivated area per management body is 2.87 ha (2017) (Ministry of Agriculture Forestry and Fisheries 2017), and ten agricultural management entities are displayed with same soil classification. Therefore, it is difficult to use the soil map in the measured resolution for regional or local management, soil management of grower's field, and land use and farming guidance at municipal level. Moreover, some growers bring soil from other places to improve the soil. Moreover, creating soil maps based on soil analysis for each plot of field becomes a subject.

The most popular visualization method is GIS software interpolation. The feature is that an arbitrary virtual data point is placed in the unmeasured area between measured data, and an estimated value calculated by interpolation methods, such as Kriging, natural neighbor, spline, and inverse distance weighting (IDW), is utilized to the virtual point, while a map drawn with smooth contour lines can be obtained. In past studies, Kriging and IDW have been often used, which are effective to grasp the variability.

IDW assumes that there are many sample points with regular arrangement, and the effect of variable decreases as the distance from the sample position increases. Then the effect of the sample data on the interpolation data is isotropic and inversely proportional to the distance.

Kriging (ordinary and universal) assumes that the distance or direction between sample points reflects a spatial correlation that can be used to explain variation in the surface. The Kriging tool fits a mathematical function to a specified number of points, or all points within a specified radius, to determine the output value for each location. It includes exploratory statistical analysis of the data, variogram modeling, creating the surface, and (optionally) exploring a variance surface. Kriging is selected when there is a spatially correlated distance or directional bias in the data.

Kriging is similar to IDW in that it weights the surrounding measured values to derive a prediction for an unmeasured location. The general formula for both interpolations is formed as a weighted sum of the data (Eq. 4.2):

$$\hat{Z}(S_0) = \sum_{i=1}^{N} \lambda_i Z(S_i) \qquad (4.2)$$

where
$Z(s_i)$ is the measured value at the ith location.
λ_i is an unknown weight for the measured value at the ith location.
S_0 is the prediction location.
N is the number of measured values.

In IDW, the weight λ_i depends solely on the distance to the prediction location. However, with the Kriging method, the weights are based not only on the distance between the measured points and the prediction location but also on the overall spatial arrangement of the measured points. To use the spatial arrangement in the weights, the spatial autocorrelation must be quantified. The weight λ_i depends on a fitted model to the measured points, the distance to the prediction location, and the spatial relationships among the measured values around the prediction location (ESRI Japan 2016; Shoji and Koike 2007).

The requirement for soil map, which is as important as understanding of variability, is providing information in a classification method capable of instantaneous decision-making. Although the interpolation method is effective for grasping variability, the interpolation methods must be determined according to the spatial arrangement of the measurement data. Also, it is hard to determine the farm work range and work amount. For the paid GIS software, the costs of introduction and maintenance are problems, and the operation procedures from converting measured data to GIS readable format for display are operational issues.

Soil mapping methods include GIS software interpolation map, gird map, and dot map. Each visualization method has its characteristics, and it is necessary to select the visualization method according to the purpose of use of the soil map. However, the purpose of use of soil map varies with growers and field managers, while some may not have a purpose of use. In addition, there are no growers who divide one plot into multiple parts and perform soil analysis and mapping according to the number of divisions. Moreover, agricultural support system for guidance and fertilization design based on high-resolution soil map has not been established.

The first use of high-resolution soil map in such situation is to grasp the variability and record the grower's awareness to facilitate the grower's decision-making. It is necessary to provide field mapping technology to provide soil maps immediately after the field observation that enables the dialogue with grower and extension instructors. If the soil map can be provided on-site, and if it can share awareness of growers, provide advice from extension instructors, and create a database of grower's decision; it will be possible to serve as a part of decision support system. Therefore, a simple GIS display function (dot map) has been developed which shows the properties requested in the visualization methods and enabled soil mapping on-site.

(3) IDW Interpolation Map

The interpolated soil map is characterized by the fact that the status of variability can be drawn with clear contour line according to the classification, so the feature can be understood immediately. But there are problems with the introduction and

maintenance cost of GIS software and the operability of the mapping procedures. ArcCatalog in ArcGIS (V10.2.2 ESRI Inc., USA), map layout software ArcMap, and extension products (Spatial Analyst et al.) were used to create interpolation map. The feature of spatial data measured by SAS is that there are plenty of data collected from one plot and there are no scattered measurement positions or extreme inhomogeneities. Therefore, the effect on the interpolation point between the measured data is assumed to be smaller as the distance from the measured data point increases, and the influence of the data acquisition location on the interpolated value is isotropic. Therefore, IDW (ESRI Japan Co. Ltd 2002) is appropriate to be adopted due to its characteristics of that the influence of the data acquisition location on the interpolation result is inversely proportional to the distance. In IDW, the output cell size, power, and search radius can be set arbitrarily, but the automatic set values by the software were used. In the interpolation method, the inner area of a point with value and location information is visualized. In order to visualize the entire field inside the boundary, it is essential to record the field edge with values (analyzed and predicted values) and location information. Since no analysis value or spectra data were acquired at the field edge, soil maps were created by replacing the value with the data point closest to the field edge based on the characteristics of IDW. In addition, to distinguish among field end points and data points, data points were indicated by " · ," and the field end points were indicated by "+" (Fig. 4.8a).

(4) Grid Map

The grid map can facilitate efficient soil management when the purpose and method of use of the soil map are determined. For example, when variable-rate spraying is manually performed using a working machine such as a broadcaster or a boom sprayer, after determination of work width of the machine, the number of travel lines, the travel route, the start and stop positions of fertilizer application, and the number of grids in the travel direction, the center of the working width is measured with SAS. The average, minimum, and maximum values are shown for each grid, and the average value is used for classification. By showing the minimum and maximum values, it is possible to grasp the variability range and check for outlier (Fig. 4.8b).

For variable-rate work based on the grid map, a fertilization map can be created with manure increasing/decreasing zones determined based on cultivation calendar and cultivation guidelines.

(5) Simple GIS display function (Dot map)

The simple GIS display function (Fig. 4.9) is a visualization method that classifies and displays measurement points with color dots. Optional features include dot size, field outline, dot color, and threshold values of up to five divisions. When the pointer cursor is placed on the memorized reference value of each soil property, statistical value (average, maximum, minimum, and coefficient of variation), and acquired data points, the absorbance, second-derivative absorbance, and prediction value are displayed. In this way, it can be determined whether a sample for soil analysis needs to be collected and whether there is an abnormal spectrum. In
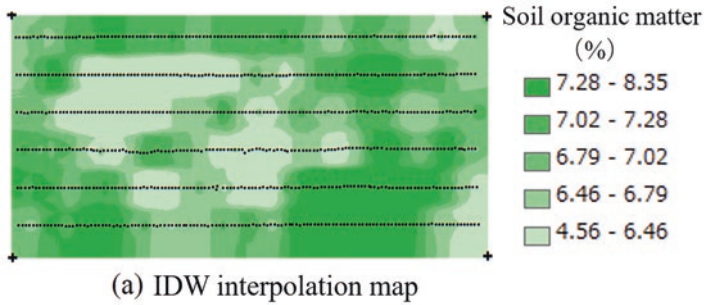
(a) IDW interpolation map
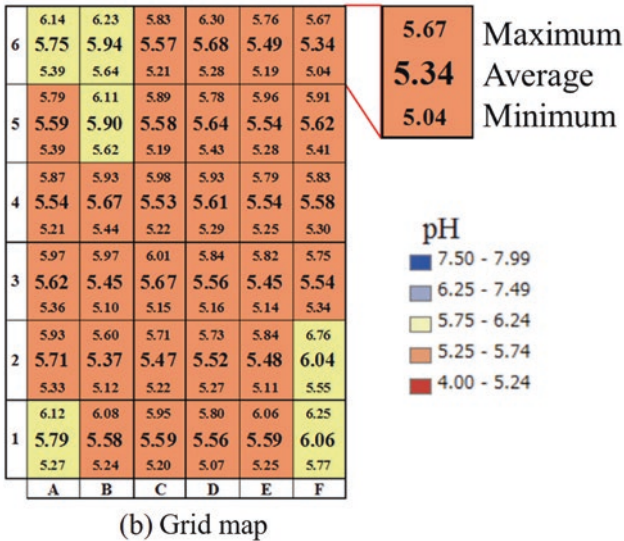
(b) Grid map

Fig. 4.8 Soil maps (**a**) IDW interpolation map (**b**) Grid map

addition, to display one plot of field or group of fields on the map, the map can dis-play an arbitrary range by zooming. By registering the position information of the field edge and the entrance of working machine, it became easy to grasp the field direction when displaying complicated shapes or multiple fields. The title of the regression coefficient is composed of identification character, property, accuracy, and range of database, to prevent selection miss and grasp reliability of the predic-tion value. By registering the regression coefficient for each property, it is possible to display the dot map immediately after field observation and reduce the cost of GIS software's introduction, which makes it possible for the growers to understand their field and make decisions on-site. The simple GIS display function has been jointly developed with the Shibuya Seiki Co., Ltd.
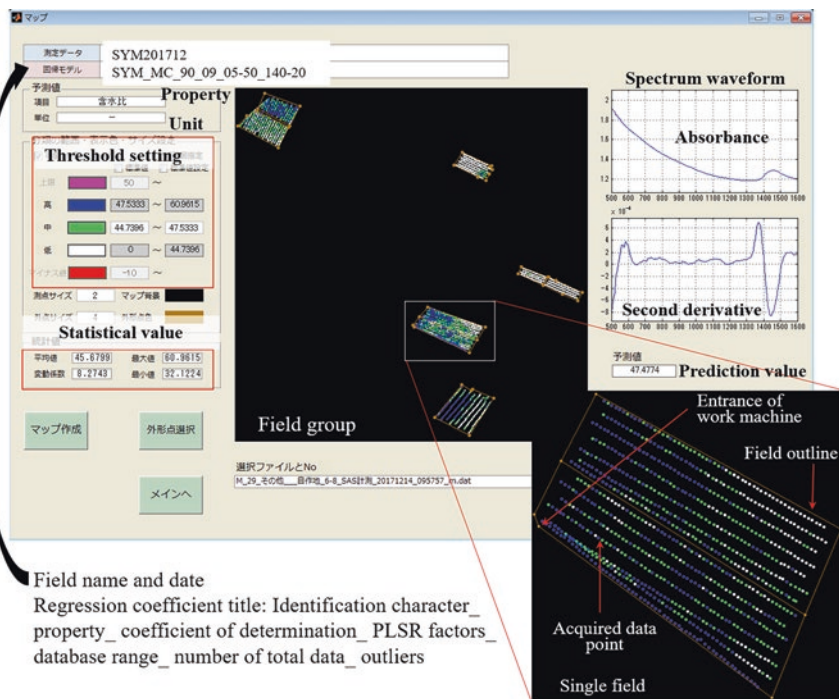
Fig. 4.9 Simple GIS display function (dot map)

4.2.2 Decision-Making for Crop Precision Farming

(1) Variable-Rate Application

(i) Test Fields, Device, and Methods

The test field was a rotation cropping field (4.43 ha, 303 m long side × 146 m short side) in Memuro-cho, Kasai-gun, Hokkaido, Japan. The test device was SAS1000, and the observation speed was 0.56 m/s, the observation depth was 0.15 m, the sampling period was 4 s, and the data measurement interval was 2.24 m. The field observation line interval was 24 m, which was the same with the pest control line. Field observations of the same field and the same line were conducted in October 2007, November 2008, and November 2010, and pH soil maps (Fig. 4.10) were provided to growers.

(ii) Make Decision by Growers

In the pH map after harvesting wheat in autumn 2007 and after harvesting sugar beet in 2008, a location with high pH value was confirmed on the south side (Fig. 4.10a, b). The grower decided to improve the soil condition before soybean
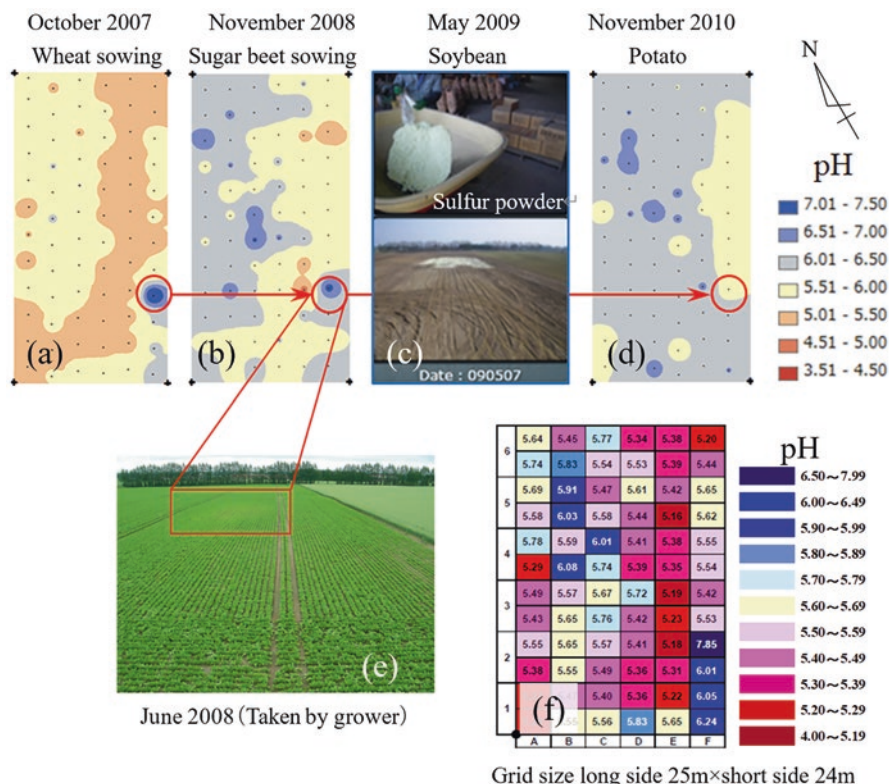
Fig. 4.10 Variable-rate application utilizing soil pH map

sowing in May 2009 and sprayed 360 kg/10a of sulfur powder by a broadcaster (Fig. 4.10c).

(iii) Reasons, Background, and Results

The high pH on the south side was because of overflowing with a large amount of lime cake (processed residue from refined sugar beet). The grower's rotation system was "wheat-sugar beet-soybean-potato-green manure," which was five crops in five years. If the pH value exceeds 6.5, potato and sugar beet may suffer disease of common scab, so the solution has been considered. In the growing season, symptoms such as slow growth and withering were visually observed in the place with high pH, and in the surrounding area, the location can be identified until harvest (Fig. 4.10e). After the harvest, the trace disappeared, and no solution was taken.

When the location with high pH can be identified from location information recorded in SAS and the grid map for easy manual variable-rate application can also be created, the grid map as shown in Fig. 4.10f can be provided. The size of the grid was determined by checking the distance over which the grower could manually adjust the spray amount. As a result of sulfur powder spraying, the field observation

after potato harvest in November 2010 confirmed that the pH dropped to 5.5–6.0 (Fig. 4.10d).

(2) Plan for Agricultural Work

(i) Test Fields, Device, and Methods

The test field was a taro rotation field (0.32 ha, 60 m long side × 54 m short side) in Aoyagi, Sayama City, Saitama Prefecture, Japan. The test device was SAS3000, and the observation speed was 0.28 m/s, the sampling period was 3 s, the observation depth was 0.15 m, and the data measurement interval was 0.84 m. For the purpose of visualizing the inside of the field with high resolution, the observation line was set at 3 m interval, to ensure that the tractor's wheel may not cover the observation line, because the interval between the taro planting rows was about 1 m and the width of the rare wheel of the tractor was 1.2 m. Field observation was conducted after taro harvest in February and December 2017. To estimate the regression coefficient for each property, a database of 100 samples for the analysis was used, which were collected in February 2017 from 10 plots of fields of 3 taro farmers in the Sayama area. For soil mapping, the soil maps with the data range divided according to the reference value of soil analysis were first provided to the grower, and then three equal division soil maps were provided.

(ii) Make Decision by Growers

The growers found that hot water extractable nitrogen and available phosphorus were below the reference value, and the exchangeable potassium was within the reference value in the divided interpolation methods (Fig. 4.11a) observed in February. It was considered that this was the topdressing effect of potassium fertilizer. From the soil map of the three equal division interpolation methods (Fig. 4.11b) observed in February, the grower changed the planting row direction from east-west to north-south.

(iii) Reasons, Background, and Work Results

The grower used sulfated potassium fertilizer as additional fertilization of the taro cultivation. The residual amount of exchangeable potassium was higher than hot water extractable nitrogen and available phosphorus, which agreed with the work of adding additional fertilizer.

According to the growers, they remembered that red soil was added to the east half of the field in the past. Also, the western taro was found to be smaller overall. The growers changed the planting row direction from east-west to north-south in consideration of cultivation management from work efficiency and soil property distribution. As a result of field observation after changing the planting row direction and after harvesting taro in December, hot water extractable nitrogen and available phosphorus were higher in the east half, while exchangeable potassium had a lower content (Fig. 4.12).

(3) Selection of Varieties Based on Differences Between Fields
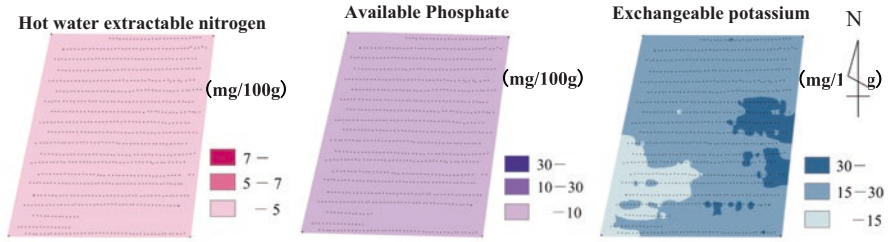
(a) Reference value division interpolation method observed in February
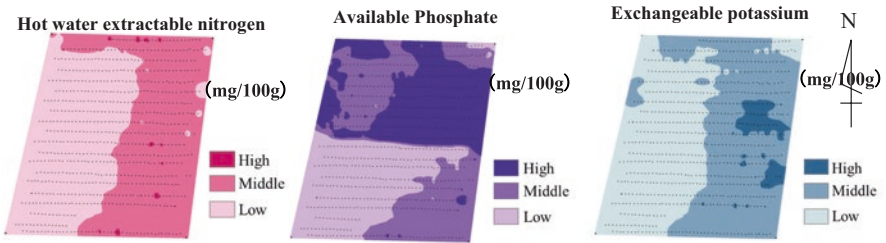
(b) Three equal division interpolation method observed in February

Fig. 4.11 Soil maps with data range (**a**) Reference value division interpolation method observed in February (**b**) Three equal division interpolation method observed in February
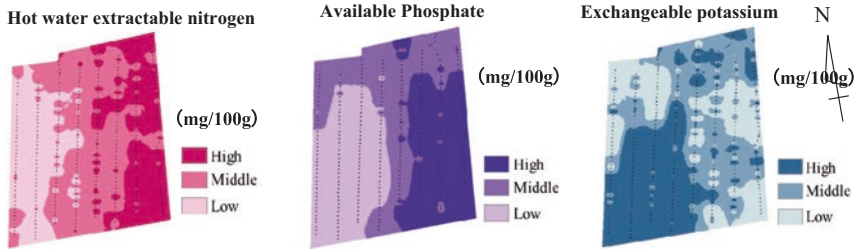
Fig. 4.12 Three equal division interpolation methods observed in December

(i) Test Fields, Device and Methods

The test fields were two plots of field (0.12 ha, 45 m long side × 30 m short side (trapezoid) and 0.16 ha, 55 m long side × 30 m short side (trapezoid)) in Aoyagi, Sayama City, Saitama Prefecture, Japan. The test device was SAS3000. The observation speed was 0.28 m/s, the sampling period was 3 s, the observation depth was 0.15 m, and the data measurement interval is 0.84 m. The interval between observation lines was 3 m; the observation line direction coincided with the direction of leveling, in north-south that crosses the direction of planting. There were factories and buildings on the west and north sides, and the location information at the end of the upper left of the two plots could not be captured accurately. Field observation was conducted after soil leveling (December 2017). To estimate the regression

coefficient for each property, the database was used in which 100 samples were collected in February 2017 at 10 plots from 3 taro farmers in the Sayama area. The soil map was confirmed with the grower after the field observation using dot maps based on the simple GIS display function of SAS3000 (Fig. 4.13).

(ii) Make Decision by Growers

Hot water extractable nitrogen

No.1

No.2

(mg/100g)

9.8～11.3   (a)

Reference value：5～7

Prediction accuracy：N=82/100, F=8

R^2_{Val}=0.83, RMSE$_{Val}$=0.84

Exchangeable potassium

(mg/100g)

40～50   (b)

N

Reference value:15～30

Prediction accuracy：N=86/100, F=6

R^2_{Val}=0.83, RMSE$_{Val}$=9.97

Available phosphate

(mg/100g)

29～41   (c)

Reference value: 10～30

Prediction accuracy：N=68/100, F=3

R^2_{Val}=0.83, RMSE$_{Val}$=5.14

Organic matter

(%)

18.0～19.5   (d)

Reference value：more than dry soil 2g per 100g（2%）

Prediction accuracy：N=84/100, F=6

R^2_{Val}=0.82, RMSE$_{Val}$=0.63

Fig. 4.13 Comparison between fields using dot map

The growers planned to cultivate Dodare (taro variety) in No. 1 field and lotus leaf in No. 2 field. But they switched the two cultivation varieties after referring to the soil maps of hot water extractable nitrogen, available phosphorus, and exchangeable potassium. So far, 2 tons of chicken manure compost has been put into the two plots of field, but it has been reduced to 1 ton.

(iii) Reasons, Background and Results

According to the growers, when the Dodare variety is cultivated in soil that is rich in nitrogen, the plant height and leaves and the mother taro tubers grow dramatically, while the secondary taro tubers tend to be small. According to the hot water extractable nitrogen soil map (Fig. 4.13a), the residual amount of both plots was higher than the reference value range, and No. 1 was higher than that of No. 2. Therefore, No.1 was planted with lotus leaves which are less affected by nitrogen.

In addition to the hot water extractable nitrogen, the residual amount of exchangeable potassium and available phosphorus in the two plots also exceeded the reference value range (Fig. 4.13b, c). Since the organic matter satisfied the condition of the standard level of 2 g per 100 g (2%) of dry soil (Ministry of Agriculture Forestry and Fisheries 2008a), the chicken manure compost input was reduced to half 1 ton.

4.3 Measurement and Application of Soil EC in Precision Agriculture

4.3.1 Soil EC Measurement: Theory and Method

Precision agriculture differentiates agriculture management based on the soil nutrient status and crop growth conditions of different locations in the farmland and can increase yield with less input. Rapid and accurate access to soil parameters is one of the bases of precision agriculture. The most informative, simple, least expensive, and accurate map of soil variability across the field is made using measurements of soil electrical conductivity (EC). Soil is an electrical conductor and soil EC is an important soil parameter. It has a relationship with several soil properties such as soil moisture, soil salinity (the amount of salt in the soil), soil texture (the percentage of sand, silt, and clay), cation exchange capacity (CEC), and organic carbon content. The measurements of the soil EC can reflect the soil status and provide a basis for implementing precision agriculture.

Soil EC is the most common measure of soil salinity and many nutrients are salts—a source of salinity. It is helpful to farmers to use soil EC to evaluate soil nutrient level. On the other hand, the nutrient accumulation, poor drainage, salt water intrusion in coastal areas, and saline irrigation water can lead to the unwanted buildup of salinity in soil, which is typically not beneficial to crops, grasses, or the microbial community in the soil. Soil salinity also affects the soil hydrology. Plant diseases and pathogens, reduced crop yields, or even crop failures may occur from

excessive soil salinity; therefore, the proper monitoring of soil salinity will help ensure the health of crops. Soil EC can change dramatically with water content and can be affected by the quality of the irrigation water, fertilization, drainage, and other natural processes. Compaction, clay content, and organic matter can influence moisture holding trends over time, also affecting EC capacities in soil.

As we know, electrical conductivity (EC), as well as its inverse electrical resistivity, is a fundamental property of a material or an object that quantifies how strongly it conducts or resists electric current. Electrical resistance is often used in electrical engineering and has the following relationship with electrical resistivity if the shape of the object is regular (Eq. 4.3):

$$R = \rho \frac{L}{S} \tag{4.3}$$

where R is electrical resistance (Ω), L is the length of the object (m), S is the cross-sectional area of the object (m^2), and ρ is the electrical resistivity ($\Omega \cdot$m).

Similarly, electrical conductance has the following relationship with electrical conductivity (Eq. 4.4):

$$G = \sigma \frac{S}{L} \tag{4.4}$$

where G is electrical conductance (Siemens, S), S is the cross-sectional area of the object (m^2), L the length of the object (m), and σ is the electrical conductivity (S/m). It is obvious that $G = (1/R)$ and $\sigma = (1/\rho)$.

From Eqs. (4.3) and (4.4), it can be seen that if the cross-sectional area and length of the measured conductor are determined, the EC of the conductor can be easily obtained. However, the soil is a half-open and infinite measuring object and is just a complex measuring object with uncertain cross-sectional area and length for the measurement of the Earth conductivity. It is impossible to measure soil EC with Eqs. (4.3) and (4.4) directly.

Soil EC depends on the concentration of conductive ions in the soil. Therefore, it can be represented by measured ion concentration in soil solution, which has linear relationship with EC of soil solution. Pore water EC or soil water EC (EC_w or σ_w) is the electrical conductivity of the water in the soil pores. In order to simply measure the EC of pore water in situ, the tiny sensors would have to be inserted into microscopic water-filled pores. Obviously, it is impossible to measure the EC of water on that scale. In fact, it is feasible to extract a soil water sample and measure the EC of that sample.

Meanwhile, saturation extract EC (EC_e or σ_e) is measured by taking a soil sample, making a saturated paste of soil and deionized water, extracting the water, and then measuring the EC of the extracted solution. However, it is not easy to measure soil EC_w or soil EC_e in a field. A soil solution method is recommended. The soil solution is prepared as following.

The soil samples collected from a farmland are air-dried, smashed, and sieved (1 mm). Then, a certain weight of air-dried soil sample is weighed and added into a test tube or measuring cup, and five times of the weight of distilled water is added into the soil sample according to the water soil ratio of 5:1. After shaking the soil water solution on an oscillator for 30 min, and then standing for 30 min, the clear soil solution or the soil solution filtered by filter paper can be directly extracted for measurement of EC. The EC of the soil solution is usually measured by electrode method. The measured EC data of soil solution is called EC_w, and the EC data measured by aforementioned method can be also called as $EC_{1:5}$, which means that the soil solution is prepared by the water soil ratio of 5:1.

Soil $EC_{1:5}$ is widely used to analyze soil salinity (He et al. 2012). Soil salinity or sodicity is thought a major impediment to sustainable agriculture, worldwide. The Songnen Plain is the second largest plain of China after and also one of the five largest salt-affected soil regions in China. Therefore, soil $EC_{1:5}$ was used to characterize the salinity and sodicity of the salt-affected soils in the Songnen Plain, China, and determine the relationships between salinity, sodicity, and cation concentrations of 1:5 extracts (Chi and Wang 2010). One hundred and twenty-one soil samples were selected to determine chemical characteristics of soil using 1:5 extraction method. All samples were air-dried and passed through a 2 mm sieve, and then 4 g of soil was taken from each sample and put into a 100 ml bottle with 20 ml distilled water. After agitated and filtered, the $EC_{1:5}$ value of the soil solution was determined by a DDS-307 conductivity meter (Shanghai Precision Scientific Instrument Co., Ltd., China). The cations Na^+, K^+, Ca^{2+}, and Mg^{2+} were determined by using inductively coupled plasma mass spectroscopy (GBC, Scientific Equipment Pty Ltd., Australia). The TCC, total cation concentration (or total soluble salt concentration) ($mmol_c$ L^{-1}), was calculated as

$$TCC = Na^+ + K^+ + Ca^{2+} + Mg^{2+} \qquad (4.5)$$

Another soil salinity parameter, sodium adsorption ratio (SAR) ($mmol_c$ L^{-1})$^{1/2}$, was calculated as

$$SAR = Na / \sqrt{\left(Ca^2 + Mg^{2+}\right)/2} \qquad (4.6)$$

The analysis results showed that the coefficients of determination (R^2) between $EC_{1:5}$ and TCC and between $EC_{1:5}$ and SAR were 0.99 and 0.87, respectively, and $EC_{1:5}$ value had higher correlation with soil parameters, TCC and SAR, and could be used to well evaluate soil salinity and sodicity.

Although soil solution EC (EC_w), including $EC_{1:5}$ and $EC_{1:1}$, can describe soil EC level to a certain extent, it cannot replace soil EC since soil in farmland is a porous medium and has three phases of solid, liquid, and gas. The EC in soil is more complex than it is in soil solution. Therefore, the bulk soil electrical conductivity (EC_b or σ_b) is proposed and applied, which is also called soil apparent electrical conductivity (EC_a or σ_a). Soil EC_a (afterward, soil EC is used instead of soil EC_a) is the

electrical conductivity of the soil/water/air matrix combined and is measured by soil sensors from the undisturbed status.

The most popular measurement method of soil EC is four-electrode method. Figure 4.14 shows the typical pattern of the four-electrode method. Two electrodes (J and K) are connected with a constant electric current source, while the other two electrodes (M and N) are connected with a voltage meter. The constant electric current is injected into soil from J and K, and then a voltage drop between M and N is detected. Using the voltage drop, the soil EC can be measured (Telford et al. 1976; Sun and Wang 2001).

Using the four-electrode method shown in Fig. 4.14, the soil EC can be calculated as the following:

$$\sigma_b = \frac{\left(\dfrac{1}{L_{JM}} - \dfrac{1}{L_{JK}}\right) - \left(\dfrac{1}{L_{KM}} - \dfrac{1}{L_{KN}}\right)}{2\pi} \frac{I}{\Delta V_{MN}} \tag{4.7}$$

where σ_b is the soil EC; L_{JM}, L_{JK}, L_{KM}, and L_{KN} are the distances between J and M, J and K, K and M, and K and N respectively; I is the electric current between J and K; and ΔV_{MN} is the voltage drop between M and N.

When $L_{JM} = L_{MN} = L_{KN} = a$, the structure of soil EC measurement method shown in Fig. 4.14 is called Wenner array, and Eq. (4.8) can be simplified as

$$\sigma_b = \frac{1}{2\pi a} \frac{I}{\Delta V_{MN}} \tag{4.8}$$

When $L_{JK} = 2a$ and $L_{MN} = b$, the structure of soil EC measurement method shown in Fig. 4.14 is called Schlumberger array, and Eq. (4.9) can be simplified as

$$\sigma_b = \frac{1}{\pi \left(\dfrac{a^2}{b} - \dfrac{b}{4}\right)} \frac{I}{\Delta V_{MN}} \tag{4.9}$$

A portable soil EC detector was developed (Li et al. 2006; Li and Li 2011). The EC detector adopts a four-electrode method and consists of three parts: a probe with four electrodes, a control and display unit, and the data processing software. The probe injects a constant electrical current into soil and detects the voltage drop

Fig. 4.14 Structure of soil EC measurement method based on four-electrode method
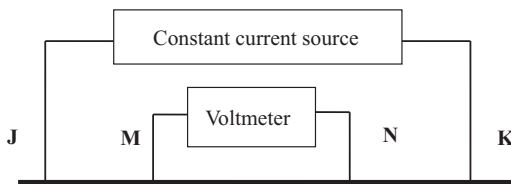
between two output electrodes. The voltage drop is then used to estimate the soil EC. The correlation analysis was performed between soil EC value and soil ammonium content, and higher correlation result was obtained ($R^2 = 0.9297$).

4.3.2 On-the-Go Measurement System of Soil EC

Soil EC, as an important parameter of soil characteristics, is of great significance to the precision management and fertilization in farmland. Precision agriculture is a differential management based on the temporal and spatial variation of agricultural parameters on the field scale. It needs modern agricultural machineries to perform the site-specific crop management. Therefore, as the one of the essential information of precision agriculture, soil EC measurement needs to be conducted rapidly, accurately, and real time. Thus, it is necessary to use the vehicle-mounted (on-the-go) measurement system to achieve the requirements of efficiency and accuracy.

(1) EM-38 Soil EC Mapping System Based on Electromagnetic Induction

The on-the-go measurement methods of the soil EC can be broadly classified into two categories, electromagnetic induction (EMI) method and aforementioned four-electrode method. EMI method is a noncontact type of method and the principal component is shown in Fig. 4.15. The instrument based on EMI method is composed of a transmitter and a receiver, placed about 1 m apart. Inside the transmitter, an alternating current (A/C) is applied to a copper coil to induce an electromagnetic wave, known as the primary magnetic field (H_T). When this magnetic field comes into contact with the conductive material such as soil, an eddy current in the soil matrix will be created. This new eddy current will generate a secondary magnetic field (H_I). Both H_T and H_I are measured by the receiver as a reinforced magnetic field (H_R). The measured response is a function of soil EC and is used to evaluate soil (Robinson et al. 2003).
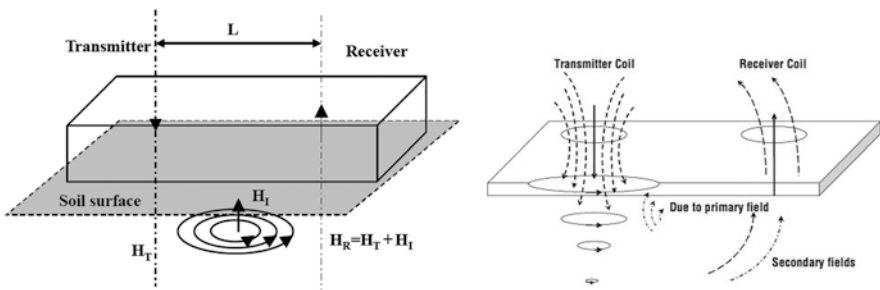
Fig. 4.15 Principal component of the EMI method

EM38 series of ground conductivity meter (Geonics Limited, Ontario, Canada)[2] is a typical soil EC measuring and mapping system. It can be used in handheld pattern and also in on-the-go pattern (vehicle-mounted) when it is equipped with a vehicle or tractor. The standard EM 38 - MK 2 includes two receiver coils, separated by 1 m and 0.5 m from the transmitter, providing data from effective depth ranges of 1.5 m and 0.75 m, respectively, when positioned in the vertical dipole orientation, and 0.75 m and 0.375 m, respectively, when in the horizontal dipole orientation, while the EM38-MK2-1 model includes one receiver coil only, at 1 m from the transmitter. The operating frequency is 14.5 kHz and measuring range is 0~1000 mS/m. External power sources can be connected to the instrument for extended field operations. When it is used in on-the-go pattern, a protective capsule, constructed of durable plastic materials, is available as an option.

A mobile data acquisition system for soil EC was developed using the Geonics EM38 sensor in order to investigate the correlation between topsoil depth and soil EC for precision agriculture (Sudduth et al. 2001). Topsoil depth is an important factor related to within-field productivity differences. The EM38 sensor was mounted on a wooden cart pulled behind a vehicle to form the mobile system with a GPS receiver and data collection computer. The test results showed that the soil EC provided the best estimates of topsoil depth and the relation between them followed the power function as Eq. (4.10):

$$y = \frac{1}{\sigma_b^{\alpha}} + \beta \qquad (4.10)$$

where y is the topsoil depth (cm), σ_b is the soil EC (mS/m), and α and β are the constants. The experiments were conducted in several farms and the model for each farm got high coefficient of determination (R^2), $R^2 = 0.84$~0.95. If α is taken as 1, the model will become easy to be applied but the accuracy will go down a little.

(2) Veris Series of Soil EC Mapping System Based on Four-Electrode Method

One widely used device to measure soil EC in the field is the Veris 3100 (3105) Soil EC Mapping System (manufactured by the Veris Technologies in Salina, Kansas), which is manufactured based on four-electrode method. The Veris 3100 EC unit (Fig. 4.16) has six disks mounted on a toolbar to act as electrodes and records soil EC readings from two different depths every second. One pair of disk electrodes induces current into the soil. The change in voltage is measured across the other two pairs of disk electrodes resulting in simultaneous EC measurements for the top 30 cm of soil (two center disk electrodes) and the top 90 cm of soil (two outside disk electrodes). A Global Positioning System (GPS) receiver is mounted on

---

[2] *Disclaimer*: Commercial products are referred to solely for the purpose of clarification and should not be construed as being endorsed by the authors or the institution with which the authors are affiliated.
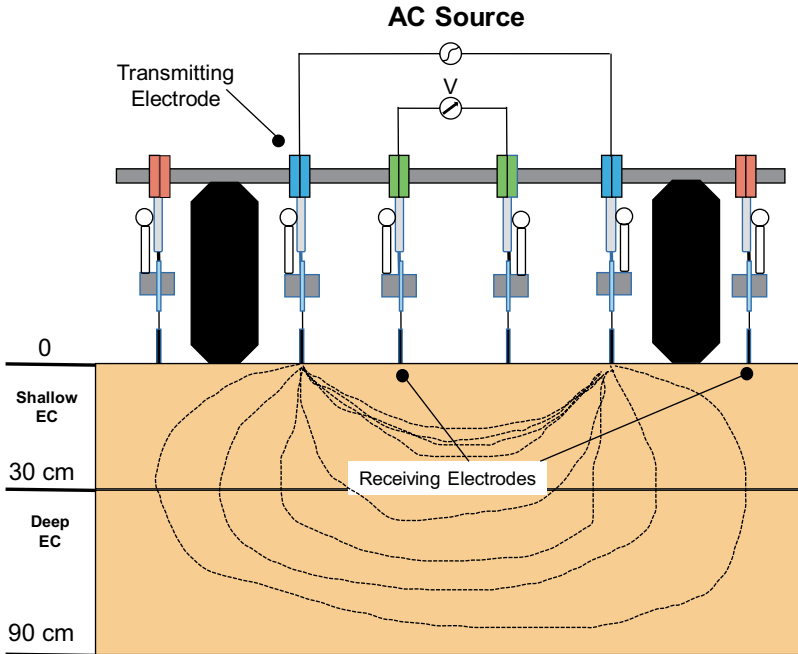
Fig. 4.16 Veris 3100 soil EC mapping system. (*Disclaimer:* Commercial products are referred to solely for the purpose of clarification and should not be construed as being endorsed by the authors or the institution with which the authors are affiliated)

the Veris unit to record the location of each soil EC measurement point in the field. All soil EC data and GPS data can be used to create a soil EC map of a field.

The differences between the soil EC zones in a field are caused by differences in the soil parameters, such as soil salinity, soil texture, soil organic matter (SOM) content, soil water content, and soil structure. It is shown that in most fields, zones with higher EC values have higher clay and organic matter content than lower EC zones. Farmers want to know the soil texture so that they can apply the correct amount of seeds, fertilizers, and irrigation to each section of their field. After understanding the pattern of soil composition across the field, farmers can make their soil and crop management decisions to fit the soil pattern rather than assuming that the whole field has a uniform composition. Soil EC maps have many economic and agronomic advantages to be used as a guide to make better management decisions. Examples of the most immediate uses of soil EC measurement and mapping are (Farahani et al. 2011) the following:

- Rapid identification of farm field variability
- Guidance to smart soil sampling as opposed to random- or grid-based soil sampling
- Logical placement and interpretation of on-farm tests

- Development of potential "management zones" for variable-rate seeding and chemical application
- Identification of coarse-textured zones within the field that are susceptible to leaching
- Identification of coarse-textured zones within the field that have low water-holding capacity and thus susceptible to crop water stress
- Identification of crop productivity zones based on relative clay and organic matter contents

Precision agriculture (site-specific management) demands the identification of subfield regions with homogeneous characteristics (management zones). However, determining subfield areas is difficult because of complex correlations and the spatial variability of soil properties and nutrient concentrations, responsible for variations in crop yields within the field. Soil EC is thought to be a potential estimator of soil properties and nutrients and a tool for the delimitation of homogeneous zones.

A Veris 3100 on-the-go soil sensing system was utilized to improve field management zone definition (Gunzenhauser et al. 2012). The Veris system with GPS is thought better to produce the dense mapping coverage needed to better define soil boundaries and improve the delineation of management zones.

Peralta and Costa (2013) also utilized a Veris 3100 on-the-go soil sensing system to delineate management zones with soil EC to improve nutrient management of crops in Argentina. The EC measurements to 0–90 cm are used because they are more stable over time than the EC measurements to 0–30 cm (Sudduth et al. 2003). The Veris 3100 sensor was pulled by a pickup truck, taking simultaneous and geo-referenced EC data in real time with a DGPS to take a satellite position once per second. Average travel speeds ranged between 7 and 11 kmh^{-1}, corresponding to about 2–3 m spacing between measurements in the direction of travel. Meanwhile, soil properties and nutrients were analyzed by means of soil sampling, including SOM, CEC, pH, NO_3^--N content, P, Zn^{+2}, Ca^{+2}, Mg^{+2}, Mn^{+2}, Na^+, K^+, Fe^{+2}, Cu^{+2}, and SO_4^{-2}. The result of PCA and ANOVA revealed that soil EC measurements successfully delimited two homogeneous soil zones associated with the spatial distribution of soil properties and some nutrients (Na^{+2}, Mg^{+2}, Mn^{+2}, Cu^{+2}, Ca^{+2}, Zn^{+2}, Fe^{+2}). These results suggest that field-scale soil EC maps have the potential to design sampling zones to implement site-specific management strategies.

Greater understanding of soil EC can offer useful information for crop management decisions. A research team at Clemson University has identified the role of soil EC in production agriculture after several years of study (Wiatrak et al. 2009). Soil texture relates to factors that have a major impact on productivity. For example, irrigation scheduling is closely related to soil type and water-holding capacity of the soil. Yield potential of sandy soils generally is less than clay soils. Variations of soil texture within a field can also have an effect on tillage decisions and pest management. Since nematode densities were highly correlated to soil texture as measured by soil EC, soil EC can be effectively used for variable-rate applications of nematicides in production fields.

It was reported that variable-depth tillage could be used to significantly reduce fuel requirements for tillage operations. Soil compaction management relies heavily on the use of annual deep tillage, usually to a uniform depth throughout the field. Soil EC data were good estimates of the topsoil thickness, and the predicted tillage depths were inversely correlated to the soil EC (Wiatrak et al. 2009).

4.3.3   Application of Soil EC in Precision Agriculture

(1) *Smart Rice Transplanter Based on Soil EC*

Smart rice transplanter is the first agricultural machine in the world to analyze soil after puddling. The smart rice transplanter could measure soil EC (apparent electrical conductivity) and topsoil depth as measurement parameters. It is very important to determine the measurement method of soil EC, soil depth, and variability map of each parameter to the smart transplant. Figure 4.17 illustrates the smart rice transplanter. The prototype was applied in eight-row-type rice transplanter (NP80, Iseki).

On-the-go measurement of soil EC is also shown in Fig. 4.17. The soil EC sensor could measure bulk electrical conductivity during rice transplanting (Morimoto et al. 2013; Morimoto and Hayashi 2017). The soil EC sensor consisted of a pair of wheel-type electrode stainless steel sensors.

Since the two electrodes of the soil EC sensor are mounted on the front wheels, the distance between the electrodes is always the same at 1.1 m. Alternative current
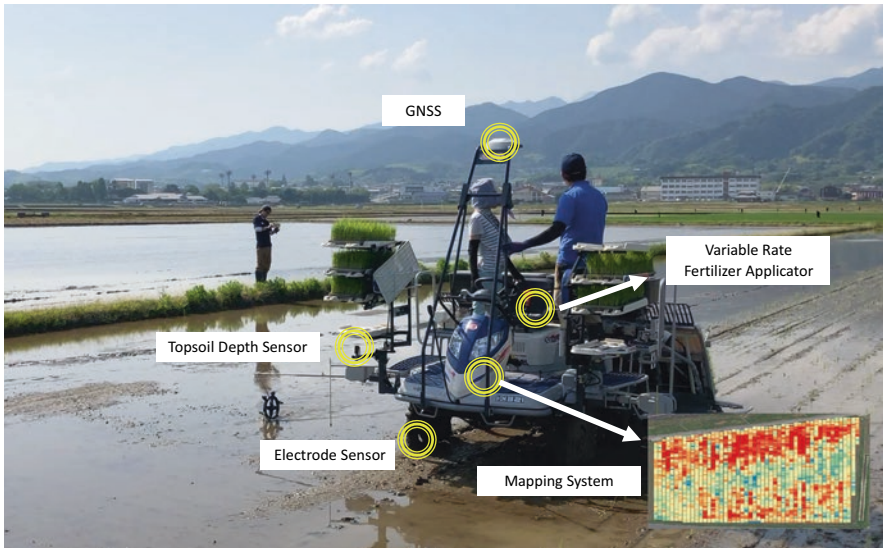
Fig. 4.17   Smart rice transplanter (Morimoto et al. 2013; Morimoto and Hayashi 2017)

of 1 kHz frequency was flowing between front wheels. Soil EC was affected by the soil moisture content and soil temperature. Since the moisture content of soil was close to 100% and solid-liquid ratio is almost 1.0 due to puddling operation, it could be measured without being affected by moisture content. In order to compensate temperature, a platinum resistance thermometer (E52, Omron) was applied. This thermometer was installed under the float of the rice transplanter to measure soil surface temperature. The interval of measurement was 1 s and the EC value was compensated to 25 °C by using Eq. (4.11):

$$\lambda_{25} = \frac{\lambda_t}{1 + 0.02(t - 25)} \tag{4.11}$$

where t is soil surface temperature (°C), λ_{25} is EC value at 25 °C (mS), and λ_t is measured electrical conductivity (mS).

Topsoil depth of paddy fields seems to be uniform, but the topsoil depth varies due to turning by agricultural machineries such as heading area. It is also known that the fertility of the soil varies due to uneven distribution of compost or soil conditioner, and these variations will result in crop lodging at the harvest time. The smart rice transplanter introduced in this section solves this lodging problem with a soil sensor and performs real-time variable fertilizer application. Topsoil depth was measured by ultrasonic distance sensor (USS, Model E4PA-LS200-MI-N, Omron). A couple of USS set in front of the rice transplanter at a height of 850 mm from the ground was shown in Fig. 4.18. Topsoil depth was calculated from a fixed height (i.e., 850 mm) minus the average of two sensor data as given by Eq. (4.12):

$$TD = 850 - \frac{\left(D_{\text{left}} + D_{\text{right}}\right)}{2} \tag{4.12}$$

where TD is the topsoil depth and D_{left} and D_{right} are the distance from left and right sensors to soil surface (mm), respectively. USS could be measured with 5 Hz interval, provided average data per five datasets.
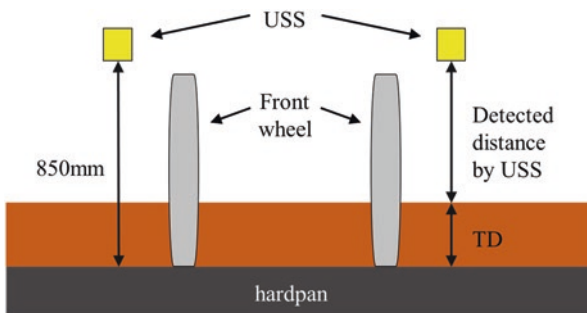
Fig. 4.18 Schematic diagram of topsoil depth sensing
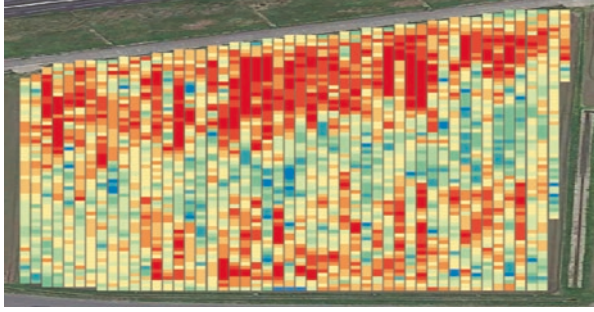
Fig. 4.19 Variability maps of soil EC (Morimoto et al. 2013; Morimoto and Hayashi 2017)

Fig. 4.20 Autonomous measurements of the soil EC based on electromagnetic induction

Figure 4.19 shows the soil EC map collected by the smart rice transplanter. Sensing and variable fertilizer application can be performed at the same time while planting rice and can be confirmed on a map immediately after the work is done. Also, as mentioned earlier, the system measures the electrical conductivity between the front wheels, so it can scan the entire field of soil. In the case of a 100 ha-scale farmhouse, a database of 1,000,000 points can be built in one year, and the number of data will increase dramatically compared to the conventional soil sampling method. It is expected that it will become the standard specification of the field with information on rice cultivation in the near future.

(2) *Topsoil Mapper Based on Soil EC*

A kind of precision agriculture equipment, Topsoil Mapper (Geoprospectors GmbH, Traiskirchen, Austria),[3] has been developed and brought to market from 2015 (http://www.geoprospectors.com/gb/). As a soil sensing product, the Topsoil Mapper (TSM) can conduct autonomous measurements of the soil EC based on electromagnetic induction as shown in Fig. 4.20. In precision agriculture,

---

[3] *Disclaimer*: Commercial products are referred to solely for the purpose of clarification and should not be construed as being endorsed by the authors or the institution with which the authors are affiliated.

differences in soil as well as varying yield capacities within a field are taken into account during the cultivation process in order to use operating materials efficiently, conserve resources, and increase agricultural yields. Using TSM, the inhomogeneity in the soil for a large area and comprehensively map soil parameters, such as soil type, water saturation, and compaction, can be obtained from the measured soil EC data. These soil parameters can then be used in real time for variable machine control.

TSM can be installed on any towing vehicle and supply exact data about soil properties. It is made of robust, entirely nonconductive material. On any towing vehicle, the TSM can be used regardless of weather and vegetation.

TSM has two working modes, BASIC and PRO.

Basic: TSM is capable of recording the depth of compaction, relative water content, and soil type automatically by using a motor during agricultural operations. In the Basic version, the user uploads the collected data via storage medium to the Data Box (cloud solution). Three maps are then produced using the parameters listed above. The data is managed centrally on the server and is available to the user at any time.

Pro: With the Pro version, the measured data is sent in real time to the terminal in the driver's cabin. In this way, the driver can immediately see, for example, the depth of compaction zones. The information is provided directly to the soil tilling machine in the form of a rule-based control. Working depth is set automatically, such that interaction with the machine's operator is not required. The advantages of this mode of operation are saving fuel and working time and reduce wear and tear due to optimized working depth.

TSM has three application possibilities, as shown in Fig. 4.20.

(i) Contact-Free Analysis of Soil Parameters

In *Basic* mode, the system can be mounted on any towing vehicle to conduct autonomous measurements of the soil EC without contacting the soil. Maps with the soil parameters for compaction, type of soil, and water saturation can be determined from the measured data. The farmers then have the option of integrating this data with other data for their farm management system and generating application maps from the results. As a rule, farmers use these maps in combination with the site-specific control of their agricultural equipment, as well as for planning of further agricultural operations.

(ii) Variable Control of Agricultural Machines in Real Time

As an alternative to asynchronous usage, the soil information can be used in *Pro* mode in combination with the appropriate agricultural equipment so that the latter can be controlled flexibly in real time. This allows two processes (acquisition and application) to be combined into one work step. When using the TSM for cultivation, the soil parameters determined by the system will be integrated into the calculation of the ideal depth of cultivation in real time. The parameters will be transferred as control parameters to the appropriate machine, while simultaneously

implementing data acquisition during the soil cultivation process. Depending on the cultivation strategy (shallow cultivation, subsoiling, or contour tracking), corresponding settings can also be modified on the terminal software so that additional information about the field will be taken into consideration.

(iii) Sensor-Supported Seed Control in Real Time

The application of sensor-supported real-time control, which can be realized with the TSM, also presents a huge potential for optimization in other areas, such as seed drilling. With this system, it is possible to adapt sowing to varying site conditions (soil type, soil moisture) in real time.

The TSM system also includes a Topsoil Visualizer (TSV), a Topsoil Data Box (TSDB), and a Topsoil Data Analyzer (TSDA).

The role of the TSV is to automatically process the recorded soil data and to calculate certain soil parameters such as compaction or water saturation. The information can then be passed directly to the implement, which automatically sets the tilling depth or controls the sowing quantity, allowing two steps to be performed simultaneously.

By the TSDB, the web portal of Geoprospectors GmbH (http://www.geoprospectors.com/gb/) allows field-related visualization of the soil parameters recorded, with the user being able to select different map displays. Output is also available as a geo-referenced dataset for further processing in the company's internal geo-information system.

The TSDA is a desktop software, which can be used to transfer the collected data to the laptop immediately and then analyze them automatically. The raw data and the processed data are displayed as maps within a few seconds. Consequently, for example, soil samples can be taken immediately and directly based on the zone maps determined on-site.

References

Adamchuk VI, Hummel JW, Morgan MT, Upadhyaya SK (2004) On-the-go soil sensors for precision agriculture. Comput Electron Agric 44:71–91

Agricultural Product Chemical Research Laboratory (2001) Soil diagnosis sheet (for field soil). https://www.nokyoren.or.jp/assay/assay-soil/. Accessed 24 Oct 2019 (In Japanese)

Akitomo I, Shimamura S (1998) Estimation of soil chemical content by near infrared spectroscopy. Bull Zootech Exp Stat Prefecture Yamaguchi Japan 14:111–117. (In Japanese)

Australian Government (2011) Carbon Credits (Carbon Farming Initiative) Act 2011. https://www.legislation.gov.au/Series/C2011A00101/Amendments. Accessed 5 May 2018

Bodun PO, Shibusawa S, Sasao A, Sakai K, Nonaka H (2000) Dredged sludge moisture prediction by textural analysis of the surface image. J Terrramech 37:3–20

Chang CW, Laird DA, Mausbach MJ, Hurburgh CR Jr (2001) Near-infrared reflectance spectroscopy-principal components regression analysis of soil properties. Soil Sci Soc Am J 65:480–490

Chi CM, Wang ZC (2010) Characterizing salt-affected soils of Songnen Plain using saturated paste and 1:5 soil-to-water extraction methods. Arid Land Res Manag 24:1–11. https://doi.org/10.1080/15324980903439362

Christy CD (2008) Real-time measurement of soil attributes using on-the-go near infrared reflectance spectroscopy. Comput Electron Agric 61:10–19

Clark DH, Mayland HF, Lamb RC (1987) Mineral analysis of forages with near infrared reflectance spectroscopy. Agron J 79(3):485–490

Dalal RC, Henry RJ (1986) Simultaneous determination of moisture, organic carbon, and total nitrogen by near infrared reflectance. Soil Sci Soc Am J 50:120–123

ESRI Japan (2016) An overview of the interpolation toolset. http://desktop.arcgis.com/ja/arc-map/10.3/tools/spatial-analyst-toolbox/an-overview-of-the-interpolation-tools.htm. Accessed 18 Nov 2017

Farahani HJ, Khosla R, Buchleiter GW (2011) Field EC mapping a new tool to make better decisions. Colorado State University Extension, Fact Sheet No. 0.568

Gunzenhauser B, Shanahan J, Lund E (2012) Utilizing on-the-go soil sensing devices to improve field management zones definition. Crop Insights 19(15):1–4

He YB, DeSutter T, Prunty L, Hopkins D, Jia XH, Wysocki DA (2012) Evaluation of 1:5 soil to water extract electrical conductivity methods. Geoderma 185–186:12–17

Hedley CB, Yule IJ (2009) Soil water status mapping and two variable-rate irrigation scenarios. Precis Agric 10:342–355

Hirota J (1999) Change of agricultural structure in rice farming and development of farmland consolidation style. J Agric Eng Soc Jpn 67(9):963–968

Imade Anom SW, Shibusawa S, Sasao A, Hirako S (2001) Soil parameters maps in paddy field using the real time soil spectrophotometer. JSAM J 63(3):51–58

Kaho T, Shibusawa S, Morimoto E, Hirako S, Ohtomo A (2004) Stability and availability of real-time soil spectrophotometer. J Jpn Soc Agric Machine 66(6):113–121. (In Japanese)

Kodaira M, Shibusawa S (2013) Using a mobile real-time soil visible-near infrared sensor for high resolution soil property mapping. Geoderma 199:64–79

Kodaira M, Shibusawa S (2016) Multivariate regression model estimation and soil mapping of multiple soil properties by using a tractor-mounted soil analyzing system. J Jpn Soc Agric Machine Food Eng 78(5):401–415. (In japanese)

Kodaira M, Shibusawa S (2018) Development of calibration model for SiO_2, Fe_2O_3, and Na_2O using subsurface diffuse reflectance spectra. J Jpn Soc Agric Machine Food Eng 80(2):114–122. (In japanese)

Kuang B, Mouazen AM (2013) Effect of spiking strategy and ratio on calibration of on-line visible and near infrared soil sensor for measurement in European farms. Soil Tillage Res 128:125–136

Kuang B, Mahmood HS, Quraishi MZ, Hoogmoed WB, Mouazen AM, van Henten EJ (2012) Sensing soil properties in the laboratory, in situ, and on-line: a review. Adv Agron 114:155–223

Li A, Li MZ (2011) Development of a ZigBee-based wireless sensor network for soil EC sensing. In: CIGR International Symposium 2011 (CIGR2011), September 19–23, 2011, Tokyo, Japan

Li M, Wang M, Wang Q (2006) Development and performance test of a portable soil EC detector. Appl Eng Agric 22(2):301–307

Malley D, Martin P, Ben-Dor E (2004) Application in analysis of soils. In: Roberts C, Workman J, Reeves III J (eds). Near infrared spectroscopy in agriculture. A Three Society Monograph (ASA, SSSA, CSSA), Madison, pp 729–784

Marín González O, Kuang B, Quraishi MZ, Munoz-García MA, Mouazen AM (2013) On-line measurement of soil properties without direct spectral response in near infrared spectral range. Soil Tillage Res 132:21–29

Matsunaga T, Uwasawa M (1992a) Near infrared diffuse reflectance spectra of the upland soils in Japan. Jpn J Soil Sci Plant Nutr 63(4):403–410. (In Japanese)

Matsunaga T, Uwasawa M (1992b) Application of near infrared spectrometry to quantitative analysis of soil physical and chemical properties. Jpn J Soil Sci Plant Nutr 63(6):712–714. (In Japanese)

Matsunaga T, Uwasawa M (1993) Near infrared diffuse reflectance spectra of clay minerals. Jpn J Soil Sci Plant Nutr 64(3):329–331. (In Japanese)

Ministry of Agriculture Forestry and Fisheries (2008a) Fundamental guidelines for fertility improvement. http://www.maff.go.jp/j/seisan/kankyo/hozen_type/h_dozyo/pdf/chi4.pdf#search=%27%E5%9C%B0%E5%8A%9B%E5%A2%97%E9%80%B2%E6%B3%95%E3%81%A8%E3%81%AF%27. Accessed 21 May 2017 (In Japanese)

Ministry of Agriculture Forestry and Fisheries (2008b) Aomori Prefecture Healthy soil making technology manual (2) Method and utilization of soil diagnosis. http://www.maff.go.jp/j/seisan/kankyo/hozen_type/h_sehi_kizyun/pdf/tuti12.pdf. Accessed 21 July 2017 (In Japanese)

Ministry of Agriculture Forestry and Fisheries (2016a) Prefectural fertilizer standards, etc.- When using fertilizer standards-. http://www.maff.go.jp/j/seisan/kankyo/hozen_type/h_sehi_kizyun/index.html. Accessed 12 Sept 2017 (In Japanese)

Ministry of Agriculture Forestry and Fisheries (2016b) Soil survey and soil collection method. http://www.maff.go.jp/j/seisan/kankyo/hozen_type/h_sehi_kizyun/pdf/gum21.pdf#search=%27%E5%9C%9F%E5%A3%8C%E8%A9%A6%E6%96%99%E6%8E%A1%E5%8F%96%E6%96%B9%E6%B3%95%27. Accessed 3 May 2018 (In Japanese)

Ministry of Agriculture Forestry and Fisheries (2017) Statistics on farmland. http://www.maff.go.jp/j/tokei/sihyo/data/10.html. Accessed 18 Nov 2017 (In Japanese)

Ministry of Foreign Affairs of Japan (2018) Sustainable Development Goals (SDGs). https://www.mofa.go.jp/mofaj/gaiko/oda/sdgs/pdf/about_sdgs_summary.pdf. Accessed 18 May 2018

Ministry of Land, infrastructure, Transport and Tourism (2018) National Land Survey (basic land survey, basic water survey) homepage. http://nrb-www.mlit.go.jp/kokjo/inspect/inspect.html. Accessed 3 May 2018 (In Japanese)

Mizuno K, Ishiguri T, Kondo T, Mizuno K (1987) Prediction of forage compositions and sheep responses by near infrared reflectance spectroscopy I. Evaluation of accuracy. Bull Natl Grassl Res Inst 38:35–47. (In Japanese)

Morimoto E, Hayashi K (2017) Design of smart agriculture Japan model. Adv Anim Biosci Precision Agric (ECPA) 8(2):713–717

Morimoto E, Hirako S, Yamasaki H, Izumi M (2013) Development of on-the-go soil sensor for rice transplanter. Eng Agric Environ Food 6(3):141–146

Mouazen AM, Baerdemaeker JD, Ramon H (2005) Towards development of on-line soil moisture content sensor using a fibre-type NIR spectrophotometer. Soil Tillage Res 80:171–183

Mouazen AM, Maleki MR, De Baerdemaeker J, Ramon H (2007) On-line measurement of some selected soil properties using a VIS-NIR sensor. Soil Tillage Res 93:13–27

Mouazen AM, Alhwaimel SA, Kuang B, Waine T (2014) Multiple on-line soil sensors and data fusion approach for delineation of water holding capacity zones for site specific irrigation. Soil Tillage Res 143:95–105

Peralta NR, Costa JL (2013) Delineation of management zones with soil apparent electrical conductivity to improve nutrient management. Comput Electron Agric 99:218–226

Robinson DA, Lesch SM, Lebron I, Shouse P (2003) Minimizing drift in electrical conductivity measurements in high temperature environments using EM-38. Soil Sci Soc Am J 68(2):339–345

Rodionov A, Welp G, Damerow L, Berg T, Amelung W, Pätzold S (2015) Towards on-the-go field assessment of soil organic carbon using Vis–NIR diffuse reflectance spectroscopy: developing and testing a novel tractor-driven measuring chamber. Soil Tillage Res 145:93–102

Roy SK, Shibusawa S, Okayama T (2006) Monitoring of topsoil characteristics using field-airborne hyperspectral signatures and underground soil images from real-time soil spectrophotometer (RTSS). J JSAM 68(2):50–62

Shibata Y (1999) Site-specific crop management for large size paddy field in Japan. J Jpn Soc Agric Machine 61(4):14–19. (In Japanese)

Shibusawa S, Hirako S, Otomo A, Li M (1999) Real-time underground soil spectrophotometer. Jpn Soc Agric Machine 61(3):131–133. (In Japanese)

Shibusawa S, Hirako S, Otomo A, Sakai K, Sasao A, Yamazaki K (2000a) Real-time soil spectrophotometer for in-situ underground sensing. Jpn Soc Agric Machine 62(5):79–86. (In Japanese)

Shibusawa S, Sato H, Hirako S, Otomo A, Sasao A (2000b) A revised soil spectrophotometer. IFAC Proc 33(29):231–236

Shibusawa S, Ehara K, Okayama T, Umeda H, Hirako S (2005) A real-time multi-spectral soil sensor: predictability of soil moisture and organic matter content in a small field. Precision Agriculture '05. Wageningen Academic Publishers, The Netherlands, pp 495–502

Shibusawa S, Kodaira M, Ninomiya K, Hirako S (2010) Commercialization of tractor-mounted soil analysis system. J Industry Acad Govern Collab 6(3):32–33. (In Japanese)

Shibuya Machinery Co. Ltd (2004) World's first new product development tractor-mounted soil analysis system. http://www.shibuya.co.jp/outline/ir/NewsReleasePDF/news20041125-1.PDF. Accessed 12 Sept 2015

Shoji T, Koike K (2007) Lecture note: Geostatistics Kring-estimation of spatial data taking account of error. J Geother Res Soc Jpn 29(4):183–194. (In Japanese)

Sudduth KA, Hummel JW (1993) Soil organic matter, CEC, and moisture sensing with a portable NIR spectrophotometer. Trans ASAE 36(6):1571–1582

Sudduth KA, Drummond ST, Kitchen NR (2001) Accuracy issues in electromagnetic induction sensing of soil electrical conductivity for precision agriculture. Comput Electron Agric 31:239–264

Sudduth KA, Kitchen NR, Bollero GA, Bullock DG, Wiebold WJ (2003) Comparison of electromagnetic induction and direct sensing of soil electrical conductivity. Agron J 95:472–482

Sun YR, Wang MH (2001) A mathematical model and its experimental study for a kind of measurement method of soil electric conductivity. Trans Chin Soc Agric Eng 17(2):20–23

Takada Y, Reon A, Nakai M, Obara H, Kohyama K (2013) Estimation of carbon and nitrogen content in surface soil horizon using "soil information web viewer". J Jpn Soc Soil Phys 123:117–124. (In Japanese)

Telford WM, Geldart L, Sheriff R (1976) Applied geophysics. Cambridge University Press, Cambridge, pp 633–640

Toriyama K (2001) Soil and plant nutrition science now developed from field study: acquisition and analysis of data from the new view point: growth of rice plant in the large size paddy field and the variability in soil nitrogen fertility. Jpn J Soil Sci Plant Nutr 72(3):483–458. (In Japanese)

Umeda T, Koyama F, Takamuku K (2001) Determination of mineral concentrations of beefs cattle manure with near infrared reflectance spectroscopy. Bull Fukuoka Agric Res Center 20:105–108. (In Japanese)

Umeda H, Shibusawa S, Okayama T, Sakuma DY, Kaho T, Ninomiya K (2011) Study of the precision farming with soil maps describing environmental load using a real-time soil sensor. J Jpn Soc Agric Machine 73(1):37–44. (In Japanese)

Viscarra Rossel RA, Walvoort DJJ, McBratney AB, Janik LJ, Skjemstad JO (2006) Visible, near infrared, mid infrared or combined diffuse reflectance spectroscopy for simultaneous assessment of various soil properties. Geoderma 131:59–75

Wiatrak P, Khalilian A, Mueller J, Henderson W (2009) Applications of soil electrical conductivity in production agriculture. Better Crops 93(2):16–17

Wojciechowski T, Czechlowski M (2013) Proximal soil sensing unit for cereal combine harvesters. Proc Inst Vehic 4(95):179–188

Yamazaki S (2008) Soil diagnosis guide. National Federation of Agricultural Cooperative Associations. Fertilizer pesticide department, Tokyo, pp 2–27. https://www.zennoh.or.jp/activity/hiryo_sehi/pdf/gijyutu_1-01b.pdf (In Japanese)

Zornoza R, Guerrero C, Mataix-Solera J, Scow KM, Arcenegui V, Mataix-Beneyto J (2008) Near infrared spectroscopy for determination of various physiCalibration, chemiCalibration and biochemiCalibration properties in Mediterranean soils. Soil Biol Biochem 40:1923–1930